

Exact Algorithms for Minimum Dilation Triangulation

Sándor P. Fekete ✉ 

Department of Computer Science, TU Braunschweig

Phillip Keldenich ✉ 

Department of Computer Science, TU Braunschweig

Michael Perk ✉ 

Department of Computer Science, TU Braunschweig

Abstract

We provide a spectrum of new theoretical insights and practical results for finding a Minimum Dilation Triangulation (MDT), a natural geometric optimization problem of considerable previous attention: Given a set P of n points in the plane, find a triangulation T , such that a shortest Euclidean path in T between any pair of points increases by the smallest possible factor compared to their straight-line distance. No polynomial-time algorithm is known for the problem; moreover, evaluating the objective function involves computing the sum of (possibly many) square roots. On the other hand, the problem is not known to be NP-hard.

(1) We provide practically robust methods and implementations for computing an MDT for benchmark sets with up to 30,000 points in reasonable time on commodity hardware, based on new geometric insights into the structure of optimal edge sets. Previous methods only achieved results for up to 200 points, so we extend the range of optimally solvable instances by a factor of 150.

(2) We develop scalable techniques for accurately evaluating many shortest-path queries that arise as large-scale sums of square roots, allowing us to certify exact optimal solutions, with previous work relying on (possibly inaccurate) floating-point computations.

(3) We resolve an open problem by establishing a lower bound of 1.44116 on the dilation of the regular 84-gon (and thus for arbitrary point sets), improving the previous worst-case lower bound of 1.4308 and greatly reducing the remaining gap to the upper bound of 1.4482 from the literature. In the process, we provide optimal solutions for regular n -gons up to $n = 100$.

2012 ACM Subject Classification Theory of computation → Computational geometry; Theory of computation → Discrete optimization; General and reference → Experimentation; Mathematics of computing → Interval arithmetic; Mathematics of computing → Arbitrary-precision arithmetic

Keywords and phrases dilation, minimum dilation triangulation, exact algorithms, algorithm engineering, experimental evaluation

Supplementary Material Code, experiment instances and results are archived on Zenodo.

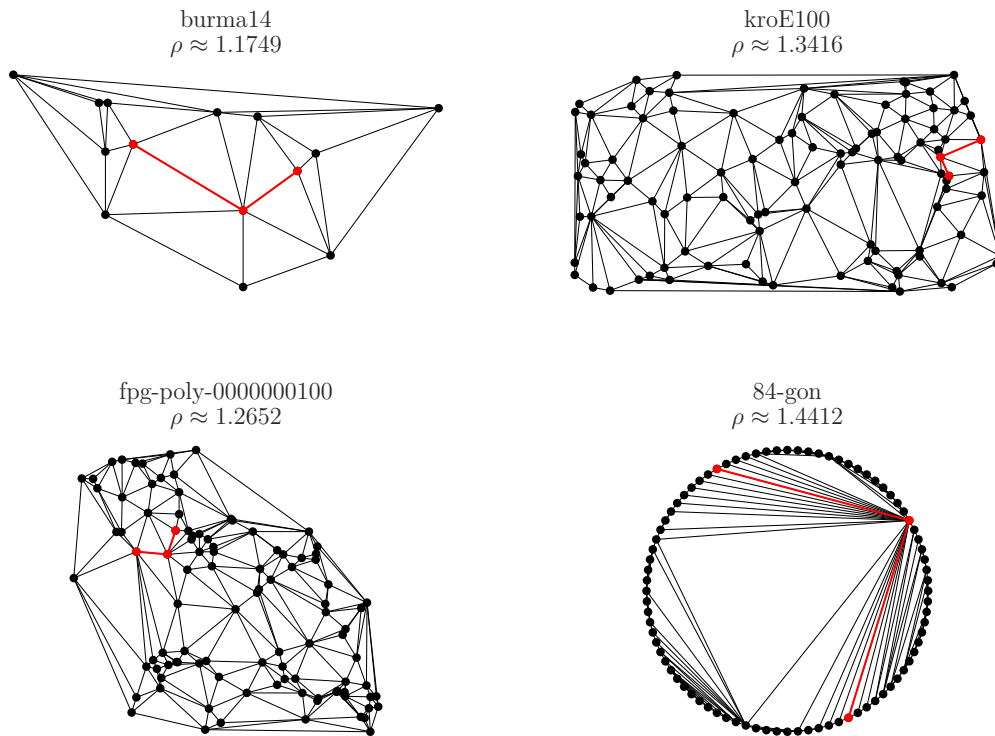
Software (Source Code): <https://doi.org/10.5281/zenodo.14266122>

Dataset (Experiment Data): <https://doi.org/10.5281/zenodo.14266122>

Funding The work presented in this paper was largely funded by the DFG grant “Computational Geometry: Solving Hard Optimization Problems” (CG:SHOP), grant FE407/21-1.

1 Introduction

Triangulating a set of points is one of the classical problems in computational geometry. On the practical side, it has natural applications in wireless sensor networks [50, 52], mesh generation [4], computer vision [47], geographic information systems [49] and many other areas [15]. On the theoretical side, finding a triangulation that is optimal with respect to some objective function has also received considerable attention: The Delaunay triangulation maximizes the minimum angle and minimizes the maximum circumcircle of all triangles.



■ **Figure 1** MDT solutions for four instances. The red edges indicate a dilation-defining path.

Minimizing the maximum edge length is possible in quadratic time [21]. On the other hand, maximizing the minimum edge length is NP-complete [27]. Famously, Mulzer and Rote [38] showed that computing the Minimum Weight Triangulation (MWT) is NP-hard.

In this paper, we provide new results and insights for another natural objective that considers triangulations as sparse structures with relative low cost for ensuing detours: The *dilation* of a triangulation T of a point set P is the worst-case ratio (among all $s, t \in P$) between the shortest s - t -path in T and the Euclidean distance between s and t . The Minimum Dilation Triangulation (MDT) problem asks for a triangulation that minimizes the dilation ρ , see Figure 1 for examples. This problem is closely related to the concept of a Euclidean t -spanner: a subgraph with dilation (also called *spanning ratio* or *stretch factor* [39]) at most t . Spanners have application in areas as robotics, network design [1, 26], sensor networks [10, 25] and design of parallel machines [3] and have been studied extensively [11]. Computing the MDT amounts to computing a *plane spanner* with smallest spanning ratio, as every plane spanner can be extended into a triangulation. For many types of triangulations, such as the Delaunay triangulation or the MWT, both lower and upper bounds on the worst-case dilation are known. Moreover, a constant upper bound on the worst-case dilation of a triangulation also implies a constant-factor approximation of the MDT. Lower and upper bounds on the worst-case dilation of the MDT have been studied, both for general point sets and for special point sets such as regular polygons or points on a circle; see Section 1.2 for further details.

Despite this importance and attention, actually computing a Minimum Dilation Triangulation is a challenging problem. Its computational complexity is still unresolved, signaling that there may not be a simple and elegant algorithmic solution that scales well.

Moreover, actually computing accurate dilations involves computing shortest paths under Euclidean distances between $\Theta(n^2)$ pairs of points requires dealing with another famous challenge [41, 18, 6, 23], as it corresponds to evaluating and comparing numerous sums of many square roots.

1.1 Our contributions

We provide various new contributions, both to theory and practice.

1. We present practically robust methods and implementations for computing an optimal MDT for benchmark sets with up to 30,000 points in reasonable time on commodity hardware, based on new geometric insights into the structure of optimal edge sets. Previous methods only achieved results for up to 200 points (involving one computational routine of complexity $\Theta(n^4)$ instead of our improved complexity of $O(n^2 \log n)$), so we extend the range of practically solvable instances by a factor of 150.
2. We develop scalable techniques for accurately evaluating many shortest-path queries that arise as large-scale sums of square roots, allowing us to certify exact optimal solutions. This differs from previous work, which relied on floating-point computations, without regard for errors resulting from numerical issues.
3. We resolve an open problem from [20] by establishing a lower bound of 1.44116 on the dilation of the regular 84-gon (and thus for arbitrary point sets). This improves the previous worst-case lower bound of 1.4308 from the regular 23-gon and greatly reduces the remaining gap to the upper bound of 1.4482 from [45]. In the process, we provide optimal solutions for regular n -gons up to $n = 100$.

1.2 Related work

The complexity of finding the MDT is unknown [24]. [29] prove that finding the minimum dilation graph with a limited number of edges is NP-hard. [12] show that finding a spanning tree of given dilation is also NP-hard. Kozma [34] proves NP-hardness for minimizing the expected distance between random points in a triangulation, with edge weights instead of Euclidean distances. For surveys, see Eppstein [24] until 2000 and [40] for more recent results.

On the practical side, the authors of [46] study the problem of finding sparse low dilation graphs for large point sets in the plane. The authors of [9] present an approximation algorithm for the related problem of improving a given graph with a budget of k edges such that the dilation is minimized. Regarding the MDT, all practical approaches in the literature are based on fixed-precision arithmetic. Klein [32] used an enumeration algorithm to find an optimal MDT for up to 10 points. The authors of [19] present heuristics for the MDT and evaluate their performance on instances with up to 200 points. Instances with up to 70 points were solved by the authors of [8] using integer linear programming techniques. In their approach, the edge elimination strategy from Knauer and Mulzer [33] was used to eliminate edges from the complete graph. Recently, Sattari and Izadi [43] presented an exact algorithm based on branch and bound that was evaluated on instances with up to 200 points.

The MDT is closely related to finding a plane t -spanner; see [35] for an overview. Chew [13] first proved an upper bound of $\sqrt{10}$ on plane t -spanners in the L_1 -metric, which he later improved [14] to 2 for the triangular-distance Delaunay graph in the plane. [5] proved that any convex point set admits a plane 1.88-spanner. For a centrally symmetric convex

point set containing n points, Sattari and Izadi [44] give an upper bound of $n/2 \sin(\pi/n)$. The best known upper bound on the dilation of arbitrary point sets is by Xia [51], who established an upper bound of 1.998 for the dilation of the Delaunay triangulation.

Mulzer [37] studied the MDT for the set of vertices of a regular n -gon and proved an upper bound of 1.48586. Amarnadh and Mitra [2] improved this bound to 1.48454 for any point set that lies on the boundary of a circle. Sattari and Izadi [45] again improved the bound to 1.4482. Dumitrescu and Ghosh [20] show that any triangulation of a regular 23-gon has dilation at least 1.4308, improving upon the bound of 1.4161 by Mulzer [37] and answering a question posed by Bose and Smit [7] as well as Kanj [31]. Dumitrescu and Ghosh [20] also computed dilations of regular 22-gon and regular 24-gon.

2 Preliminaries

Let $P \subset \mathbb{R}^2$ be a set of points in the plane. We denote the Euclidean distance between two points $u, v \in P$ by $d(u, v)$. For a connected geometric graph $G = (P, E)$ with $E \subseteq \binom{P}{2}$, we denote the Euclidean shortest path between two points $u, v \in P$ by $\pi_G(u, v)$ and its length by $|\pi_G(u, v)|$, omitting G if it is clear from context. The dilation $\rho_G(u, v)$ between two points u, v in G is the ratio $\rho_G(u, v) := \frac{|\pi_G(u, v)|}{d(u, v)}$ between the shortest path length and the Euclidean distance. The dilation $\rho(G)$ of the graph G is defined as the maximum dilation between any two points in P , i.e., $\rho(G) := \max\{\rho_G(u, v) \mid u, v \in P, u \neq v\}$.

In the remainder of this work, the graph G we consider is a triangulation, i.e., a maximal crossing-free graph on P . Two edges $e_1 = (p_1, q_1), e_2 = (p_2, q_2)$ are said to *cross* or *intersect* iff the line segments they induce intersect in their interior. Given a point set P , the Minimum Dilation Triangulation problem (MDT) asks to find a triangulation T of P minimizing $\rho(T)$.

3 Candidate edge enumeration

Here we describe a novel and practically efficient scheme for enumerating a set of edges that induces a supergraph of the MDT. We start with the underlying theoretical ideas for this supergraph, followed by an algorithm for computing a supergraph of any triangulation with dilation *strictly less* than a given bound ρ , which we exploit to enumerate a supergraph of the MDT with a (usually) small number of edges. This is further adapted to reductions of the dilation bound ρ . We also discuss the computation of lower bounds on the dilation of the MDT. We defer the discussion of some implementation details to Appendix A.

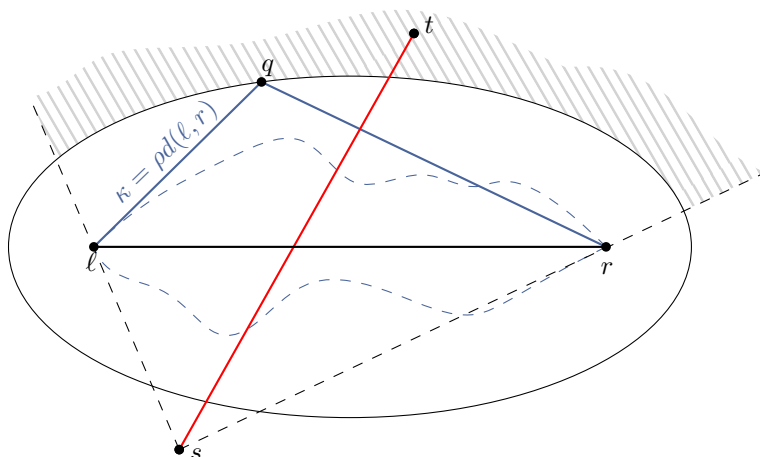
3.1 Theoretical background

Our supergraph is based on the well-known *ellipse property* (used in [8, 29, 33]) that all edges of a triangulation T with dilation below ρ must satisfy.

► **Definition 1.** *A pair of points s, t has the ellipse property with respect to a point set P and a dilation bound ρ if, for any pair of points $\ell, r \in P \setminus \{s, t\}$ such that ℓr and st intersect, $\min\{d(\ell, s) + d(s, r), d(\ell, t) + d(t, r)\} < \rho d(\ell, r)$.*

Recall that the set of points that have the same sum of distances κ to two points ℓ, r with $\kappa \geq d(\ell, r)$ is an *ellipse* with ℓ, r as its focal points (or *foci*); thus, all paths between ℓ and r with length less than $\kappa = \rho \cdot d(\ell, r)$ must lie strictly inside this ellipse.

If a pair of points s, t does not have the ellipse property, then there is a pair of points ℓ, r such that st cuts through all paths between ℓ and r that could have dilation less than ρ ; see Figure 2. We call such a pair of points ℓ, r an *exclusion certificate* for s, t .



■ **Figure 2** Any path connecting ℓ and r with length below $\kappa = \rho d(\ell, r)$ must lie within the ellipse (dashed black lines). The edge st does not have the *ellipse property* as neither s nor t lie inside the ellipse; therefore, inserting st makes connecting ℓ and r by a sufficiently short path impossible.

► **Observation 2.** Let $\rho \geq 1$ be some dilation bound and let T be a triangulation containing the edge st for points s, t that do not have the *ellipse property* w.r.t. P and ρ . Then, $\rho(T) \geq \rho$.

3.2 High-level description

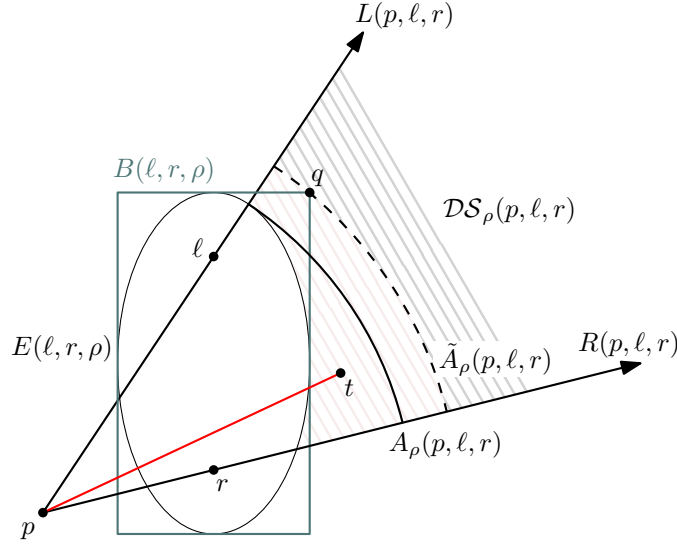
Preliminary experiments showed that a brute-force check of each of the $\Theta(n^4)$ pairs of potential edges is impractical for large n , dominating the overall runtime time even for early versions of our solution approach.

We therefore developed a more efficient scheme to enumerate a superset of the edges that satisfy the ellipse property. This scheme performs a *filtered incremental nearest-neighbor search* from each point $p \in P$ to identify all candidate edges of the form pt , i.e., looking for all possible *neighbors* t of p . This search is efficiently implemented on a quadtree containing all points. While enumerating candidates, we construct so-called *dead sectors*, i.e., regions of the plane that cannot contain possible neighbors of p . We exclude all points that lie in dead sectors; we also use dead sectors to prune entire nodes of the quadtree and to terminate the search early if it has become clear that all remaining points must be in a dead sector. This usually avoids considering most points as potential neighbors of p individually. The algorithm has a runtime of $O(nk \log n)$, where k is the average number of points and quadtree vertices considered individually from each point. At worst, this can be $O(n^2 \log n)$; in practice, k is often much lower than n . A related, slightly less complex enumeration algorithm applied to minimum-weight triangulations by Haas [30] scales to 10^8 points. In the following, we describe the components of the enumeration scheme in more detail.

3.3 Dead sectors

We begin by giving a definition of the dead sectors we use.

► **Definition 3.** Given a dilation ρ , a source point p and two points ℓ, r , the dead sector $\mathcal{DS}_\rho(p, \ell, r) \subset \mathbb{R}^2$ is the region of all points t such that pt intersects ℓr and neither p nor t lie in the ellipse with foci ℓ, r and focal distance sum $\kappa = \rho d(\ell, r)$.



■ **Figure 3** A dead sector $\mathcal{DS}_\rho(p, \ell, r)$, shaded in gray and red with the ellipse $E(\ell, r, \rho)$. We approximate the ellipse by a disk centered at p with radius $\tilde{A}_\rho(p, \ell, r)$ (thereby ignoring the red area), which is the distance from p to the farthest point q of the rectangle $B(\ell, r, \rho)$ in $\mathcal{DS}_\rho(p, \ell, r)$.

Depending on p , ρ , ℓ and r , $\mathcal{DS}_\rho(p, \ell, r)$ is either empty (if p is in the ellipse) or it is bounded by two rays and an elliptic arc; see Figure 3. In that case, it can also be interpreted as an elliptic arc and an interval of polar angles around p .

During our enumeration we construct many dead sectors, the union of which can become quite complex, making it cumbersome and inefficient to work with directly. We instead chose to simplify the shape of our dead sectors, giving up a small fraction of excluded area in exchange for a simple and efficient representation. We replace the elliptic arc by a single disk centered on p , whose radius is at least the maximum distance from p to any point on the elliptic arc. We can hence represent each non-empty simplified dead sector by a polar angle interval around p and a single radius called *activation distance* $A_\rho(p, \ell, r)$; see Figure 3.

We initially attempted to compute fairly precise upper bounds on the approximation distance; however, due to computational and numerical issues described in Appendix A.1.1, we decided to use a more robust and efficient approach. Instead of using the elliptic arc, we compute an upper bound $\tilde{A}_\rho(p, \ell, r)$ using a minimal rectangle $B(\ell, r, \rho)$ containing the ellipse with sides are parallel and perpendicular to ℓr . We only need to check the extreme points of $B(\ell, r, \rho)$ and its intersections with the rays $L(p, \ell, r)$ and $R(p, \ell, r)$ to compute an upper bound $\tilde{A}_\rho(p, \ell, r)$; see Figure 3.

In the worst case, these simplifications may lead to additional candidate edges. While this cannot make the resulting graph exclude any edges that satisfy the ellipse property, it is still undesirable; we use additional checks for further reductions later on.

3.4 Quadtree

We use a quadtree containing all points in P for the filtered incremental search. The points are stored in a contiguous array A_P outside the tree. Each quadtree node v is associated with a contiguous subrange of A_P represented by two pointers. This subrange contains the points in the subtree \mathcal{T}_v rooted at v . Each node also has a bounding box that contains all points in \mathcal{T}_v . Each interior node has precisely four children; each leaf node contains at

most a small constant number of points. To allow the contiguity of the subranges, points are reordered during tree construction. This has the added benefit of spatially sorting the points, improving the probability that geometrically close points are near each other in memory [30].

3.5 Enumeration process

One can think of the filtered incremental search from p as a process of continuously growing a disk centered at p starting with a radius of 0. As in the sweep-line paradigm, one encounters different types of events at discrete disk radii. We primarily encounter events when the disk first touches a point of P or the bounding box of a quadtree node.

Observe that, during a search from a point p , the dead sectors have two states: either their activation distance is not yet reached, in which case they are *inactive* and do not exclude any points, or they are *active* and exclude all points in a certain polar angle interval around p . We therefore also introduce events when the disk radius reaches the activation distance of a dead sector. This enables efficient management of active dead sectors as a set of polar angle intervals around p ; we discuss ensuing numerical issues in Appendix A.3.

When we first encounter a point t , we have to determine whether t is in any dead sector by checking the active dead sector data structure. If it is not, we have to report it as potential neighbor of p , adding it to a set of points sorted by polar angle around p . Furthermore, to construct new dead sectors, we combine t with $O(1)$ other points of P ; which points we use is decided by a heuristic discussed in Appendix A.1.

When we encounter a quadtree node v , we have to determine whether v 's bounding box is fully contained in the union of all dead sectors and can thus be pruned; we thus again check the active dead sectors. Otherwise, we have to take v 's children, or the points it contains if it is a leaf, into account; they are then considered as future events.

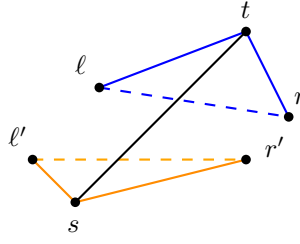
3.6 Initialization and postprocessing

We initially compute the Delaunay triangulation of the point set P and compute its dilation. We also optionally attempt to improve the dilation of the triangulation by a simple improvement heuristic. The heuristic is based on computing constrained Delaunay triangulations, greedily adding shortcut edges as constraints to reduce the length of the path currently defining the dilation. We then use the resulting dilation ρ as bound for the enumeration process outlined in the previous sections, enumerating only edges that could locally be in a triangulation with dilation strictly below ρ .

After the initial enumeration process is complete, we are left with a set of *possible* edges and can safely ignore all other edges. We postprocess these as follows. For each possible edge pq , we compute the set of possible edges intersecting it. We need this information later on to model the problem of finding a triangulation on the set of possible edges. For each pair st, lr of intersecting edges, we explicitly check whether either pair is an exclusion certificate for the other. In many cases, this postprocessing gets us very close to the edge set that would be obtained by the trivial $\Theta(n^4)$ edge candidate enumeration algorithm; see the experiment section for details. We mark each edge that does not have intersecting possible edges as *certain*; certain edges must be part of any triangulation with dilation less than ρ .

3.7 Dilation thresholds

We also compute a *dilation threshold* $\vartheta(st)$ for each possible edge st . Let $I(st)$ be the set of possible edges intersecting st . For each $lr \in I(st)$, we can compute a lower bound on the



■ **Figure 4** If st (black) is present, the pairs ℓ, r (resp. ℓ', r') can only be connected by paths that have at least the length of the solid blue (resp. orange) path. Hence, the ratio between the solid and dashed blue (resp. orange) paths is a lower bound on the dilation of any triangulation containing st . The maximum of such lower bounds for st is the dilation threshold $\vartheta(st)$ of st .

dilation of the shortest path connecting ℓ to r , should st be present, as

$$\rho_{st}(\ell r) = \min\{d(\ell, s) + d(s, r), d(\ell, t) + d(t, r)\} / d(\ell, r);$$

see Figure 4. The dilation threshold of st is then $\vartheta(st) = \max_{\ell r \in I(st)} \rho_{st}(\ell r)$.

► **Observation 4.** *If an edge st has dilation threshold $\vartheta(st)$, it is not in any triangulation with dilation $\rho < \vartheta(st)$.*

This allows us to quickly exclude further edges if we lower the dilation bound ρ we aim for, without reenumerating edges or recomputing intersections.

3.8 Lower bounds

We use the dilation thresholds to bound the minimum dilation. For each edge st , either st or some edge crossing it must be in any triangulation. Thus, the minimum of all dilation thresholds among $\{st\} \cup I(st)$ is a lower bound on the minimum dilation. Combining all edges, we obtain the following lower bound:

$$\rho(T) \geq \max_{st} \min\{\vartheta(pq) \mid pq \in \{st\} \cup I(st)\}.$$

We use interval arithmetic to compute a safe lower bound on this value in $O(1)$ time per intersection between two edges resulting from our enumeration.

Furthermore, by computing the points on the convex hull, we also know the number of edges g of any triangulation. This also gives us a lower bound on the minimum dilation by considering the g lowest dilation thresholds. We also use Kruskal's algorithm to compute the lowest dilation threshold that admits a connected graph.

4 Exact algorithms

Now we present two exact algorithms: INCMDT is an incremental method that uses a SAT solver for iterative improvement, until it can prove that no better solution exists. BINMDT is based on a binary search for the optimal dilation ρ ; once the lower and upper bound are reasonably close, the approach falls back to INCMDT to reach a provably optimal solution.

4.1 Triangulation supergraph

Both algorithms rely on the MDT supergraph mentioned in Section 3. As part of this computation, we also obtain an initial triangulation and its dilation, as well the intersecting

possible edges $I(st)$ for each possible edge st . In both algorithms, we may gradually discover triangulations with lower dilation; these are used to exclude additional edges using the precomputed dilation thresholds $\vartheta(e)$. To keep track of the status of each edge, we insert all points and possible edges into a graph data structure we call *triangulation supergraph*. In this structure, we mark each edge as *possible*, *impossible* or *certain*. Initially, all enumerated edges are *possible*. If, at any point, all edges intersecting an edge e become *impossible*, e becomes *certain*. If an *impossible* edge becomes *certain* or vice versa, the graph does not contain a triangulation any longer. If this happens, we say we encounter an *edge conflict*.

4.2 SAT formulation

Given a triangulation supergraph $G = (P, E)$, we model the problem of finding a triangulation on *possible* and *certain* edges using the following simple SAT formulation. Let $E_p \subseteq E$ be the set of non-*impossible* edges when the SAT formulation is constructed. For each edge $e \in E_p$, we have a variable x_e . We use the following clauses in our formulation.

$$\neg x_{e_1} \vee \neg x_{e_2} \quad \forall e_1, e_2 \in E_p : e_2 \in I(e_1) \quad (1)$$

$$x_e \vee \bigvee_{e_j \in I(e)} x_{e_j} \quad \forall e \in E_p \quad (2)$$

Clauses (1) ensure crossing-freeness and clauses (2) ensure maximality. When an edge e becomes certain, we add the clause x_e ; similarly, when an edge becomes impossible, we add the clause $\neg x_e$. Both algorithms are based on this simple formulation; in the following, we describe how they use and modify it to find an MDT.

4.3 Clause generation

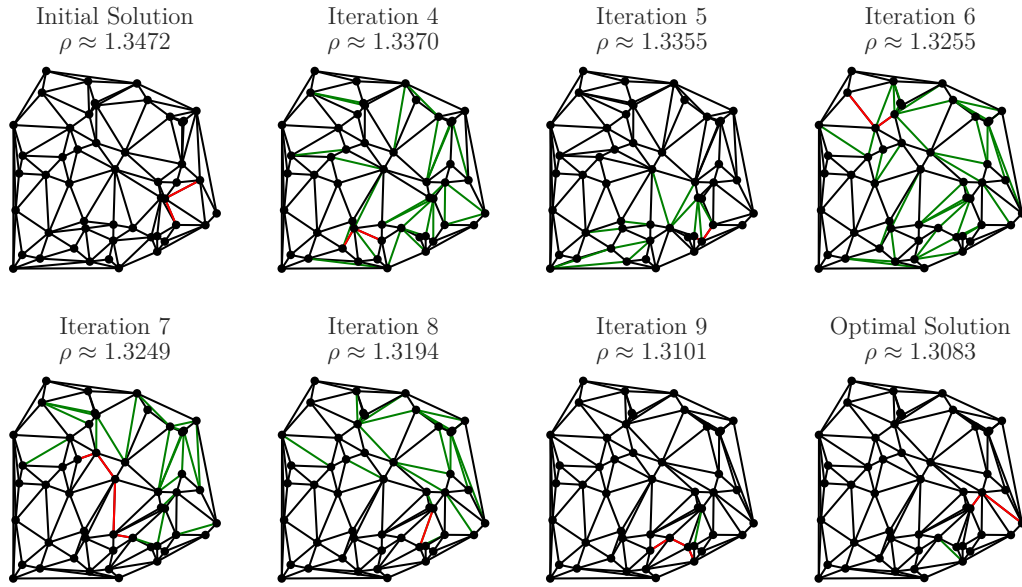
The following subproblem, which we call *dilation path separation*, arises in both our algorithms: Given a dilation bound ρ , a triangulation supergraph $G = (P, E)$ excluding only edges that cannot be in any triangulation with dilation less than ρ , a current triangulation T and a pair of points $s, t \in P$ such that $|\pi_T(s, t)| \geq \rho \cdot d(s, t)$, find a clause C that is (a) violated by T and (b) satisfied by any triangulation T' with $\rho(T') < \rho$.

► **Lemma 5.** *Assuming a polynomial-time oracle for comparing sums of square roots, there is a polynomial-time algorithm that solves the dilation path separation problem.*

Proof. Let Π be the set of all s - t -paths π in G with $|\pi| < \rho \cdot d(s, t)$. We begin by observing that, along every path $\pi \in \Pi$, there is an edge $e \in E$ that is not in T ; otherwise, we get a contradiction to $|\pi_T(s, t)| \geq \rho \cdot d(s, t)$. Let $E' \subseteq E \setminus T$ be a set of edges such that for each $\pi \in \Pi$, there is an edge $e \in E'$ on π . Then, $C = \bigvee_{e \in E'} x_e$ is a clause that satisfies the requirements; note that if Π is empty, the empty clause can be returned.

T contains no edge from E' , so C is violated by T . Furthermore, if a triangulation T' with $\rho(T') < \rho$ does not contain any of the edges in E' , it contains none of the paths in Π . Therefore, $\pi_{T'}(s, t)$ uses an edge that is not in E , which has been excluded from all triangulations with dilation less than ρ ; a contradiction. E' can be computed by repeatedly computing shortest s - t -paths π ; as long as $|\pi| < \rho d(s, t)$, we find an edge $e \notin T$ on π , add e to E' and forbid it in future paths. The number of edges bounds the number of iterations of this process; using the comparison oracle, we can efficiently perform each iteration. ◀

For a description of how we compute E' in practice, see Appendix A.2.1.



■ **Figure 5** Progress of the incremental algorithm on an instance with $n = 50$ points. Green edges indicate changes in the triangulation, red edges indicate a dilation-defining path.

4.4 Incremental algorithm

Based on the SAT formulation and the algorithm for the dilation path separation problem, INCMDT is simple. Given an initial triangulation T with dilation ρ , we enumerate the set of candidate edges and construct a triangulation supergraph G with bound ρ . We construct the initial SAT formula M and solve it; if it is unsatisfiable, the initial triangulation is optimal. Otherwise, we repeat the following until the model becomes unsatisfiable or we encounter an edge conflict, keeping track of the best triangulation found, see Figure 5.

We extract the new triangulation T' from the SAT solver and compute the dilation ρ' and a pair s, t of points realizing ρ' . If ρ' is better than the best previously found dilation ρ , we update ρ and mark all edges e with $\vartheta(e) \geq \rho'$ as *impossible*. We then set $T = T'$ and solve the dilation path separation problem for ρ, G, T, s and t . We add the resulting clause to M and let the SAT solver find a new solution.

4.5 Binary search

Preliminary experiments with INCMDT showed that we spend almost all runtime for computing dilations, even for instances for which we could rely exclusively on interval arithmetic, requiring no exact computations. For many instances, most iterations of INCMDT resulted in tiny improvements of the dilation. To reduce the number of iterations (and thus, dilations computed), we considered the binary search-based algorithm BINMDT.

4.5.1 High-level idea

At any point in time, aside from the dilation ρ_{ub} of the best known triangulation, BINMDT maintains a lower bound ρ_{lb} on the dilation, initialized as described in Section 3.

As long as $\rho_{\text{ub}} - \rho_{\text{lb}} \geq \sigma$ for a small threshold value σ , BINMDT performs a binary search. It computes a new dilation bound $\rho = \frac{1}{2}(\rho_{\text{lb}} + \rho_{\text{ub}})$. It then uses the SAT model in

a similar way as INCMDT to determine whether a triangulation T with $\rho(T) < \rho$ exists. If it does, it updates $\rho_{\text{ub}} = \rho(T)$; otherwise, it updates $\rho_{\text{lb}} = \rho$.

Once $\rho_{\text{ub}} - \rho_{\text{lb}}$ falls below σ , BINMDT falls back to a slightly modified version of INCMDT to find the MDT, starting from the best known triangulation with dilation ρ_{ub} .

In the following, we describe and motivate the differences between how INCMDT and BINMDT use the SAT formulation; for more details, see also Appendix A.2.2.

4.5.2 Dilation sampling

To further reduce the time spent on computing dilations, observe the following. When a node v of some graph G is expanded in Dijkstra’s algorithm from source s , we know the shortest path from s to v and thus the dilation $\rho_G(s, v)$. Because $\rho_G(s, v) \leq \rho(G)$, we can compute a lower bound on the dilation much faster than the precise value by only performing a constant number of node expansions from each point $p \in P$. We call this *sampling* of the dilation. Given a bound ρ on the dilation, we can sample a triangulation T for violations, i.e., pairs s, t of points with $\rho_T(s, t) \geq \rho$. We observed that a dilation-defining path usually consisted of few edges; thus, we have a good chance of finding it by sampling.

If it is likely that a new-found triangulation T' violates a given bound ρ , we can thus expect to save time by sampling for violations instead of computing the dilation exactly. Sampling also allows us to use multiple violations to construct multiple clauses in each iteration, potentially further reducing the number of iterations. BINMDT uses sampling after each SAT call with a small constant limit on the number of violations. If violations are found, no full dilation computation is required and violations are used to construct clauses. Only if no violations are found, we compute the exact dilation; ideally, this only happens once for each upper bound reduction in the binary search, namely once we find a triangulation satisfying the current bound. We also sample in the final improvement phase of BINMDT. For an experimental overview on the number of times sampling was sufficient in comparison to the number of times the dilation had to be computed exactly, see Appendix B.1.

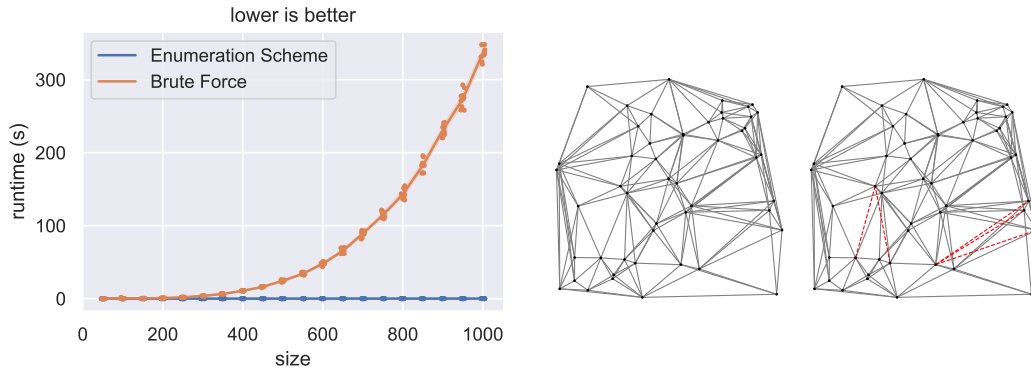
5 Empirical evaluation

Now we present experiments to evaluate our algorithms. We used Python 3.12, with a core module written in C++20 for all computationally heavy tasks; the code was compiled with GCC 13.2.0 in release mode. We use CGAL 5.6.1 for geometric primitives and exact number types, Boost 1.83 for utility functions and pybind11 2.12 for Python bindings and use the incremental SAT solver CaDiCaL 1.9.5 via the PySAT interface for solving the SAT models. All experiments were performed on Linux workstations equipped with AMD Ryzen 9 7900 CPUs with 12 cores/24 threads and 96 GiB of DDR5-5600 RAM running Ubuntu 24.04.1.

5.1 Research questions

Our experimental evaluation aims to answer the following questions.

- Q1 How does the edge enumeration algorithm from Section 3 compare to the brute force enumeration in terms of runtime and the number of edges eliminated? Can we solely rely on this algorithm or should we reconsider using the brute force enumeration?
- Q2 What is the quality of the initial solutions computed by the Delaunay triangulation and the constrained Delaunay triangulations from Section 3 compared to the optimal solution?



■ **Figure 6** Comparison of our approach from Section 3 and the $\Theta(n^4)$ brute force elimination on the *random* instance set. **(Left)** The $\Theta(n^4)$ elimination is infeasible for larger instances. **(Right)** In all cases, only a small number of (red) edges were not eliminated by our approach.

- Q3 How do our approaches compare to existing algorithms for the MDT w.r.t. runtime and solution quality? Can we solve instances with thousands of points to provable optimality?
 Q4 How do BINMDT and INCMDT compare? Which should be used for large instances?

5.2 Experiment design

To answer our questions, we collected and generated a large set of instances, consisting of instances from the following instance classes. In all cases, the coordinates of points in the instances are either integers or double precision floating-point numbers.

random-small We include instances from the work of [8]. The 210 instances have fixed sizes $n \in \{10, 20, \dots, 70\}$ and were generated by placing uniformly random points inside a 10×10 square. For each size a total of 30 instances were generated.

random We include two sets of randomly generated instances. These encompass a set of instances with points with float coordinates chosen uniformly between 0 and 10^3 , ranging from 50 to 10,000 points. This resulted in a total of 800 instances.

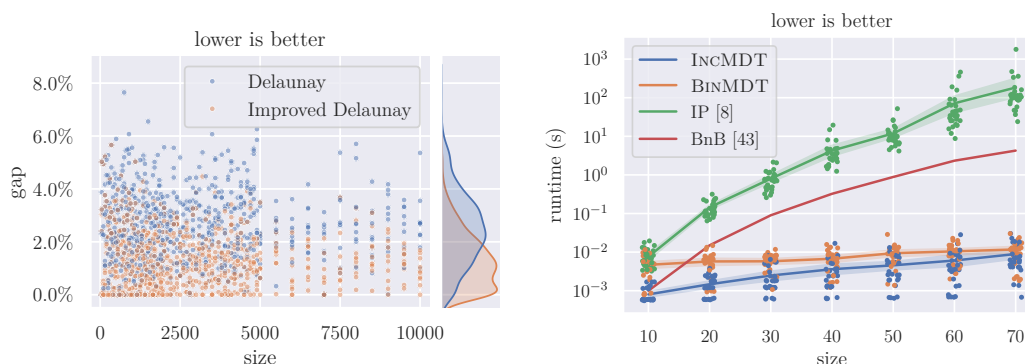
public We include instances from all well-known publicly available benchmark instance sets we could locate. These include point sets previously used in the CG:SHOP challenges [17, 16], TSPLIB instances [42], instances from a VLSI dataset¹ and point sets from the Salzburg Database of Polygonal Inputs [22]. In total, we collected 486 instances with up to 10,000 points and an additional 38 with up to 30,000 points.

5.3 Q1: Edge enumeration

We first compare the edge enumeration algorithm from Section 3 to the $\Theta(n^4)$ brute force enumeration of all possible edges on the *random* instance set. Both preprocessing options include finding all pairwise intersections between the enumerated segments. Due to the $\Theta(n^4)$ runtime, we only consider instances with up to 1000 points; see Figure 6.

The $\Theta(n^4)$ algorithm precisely identifies all edges that have the ellipse property; it can hence only eliminate more edges than the edge enumeration algorithm from Section 3. However, for our test instances, the number of edges that can be eliminated by our approach is

¹ <https://www.math.uwaterloo.ca/tsp/vlsi/index.html>



■ **Figure 7 (Left)** Initial solution comparison on the *random* set with up to 10,000 points. Delaunay triangulations can be improved by shortcut edges, but are often close to the optimal solution. **(Right)** Runtime comparison with the approaches from [8] and [43] on the *random-small* set.

almost identical to the $\Theta(n^4)$ algorithm; see Figure 6 for an example. The runtime makes the $\Theta(n^4)$ algorithm infeasible for larger instances; it takes more than 250s for instances with only 1000 points, compared to < 1 s for our more efficient approach.

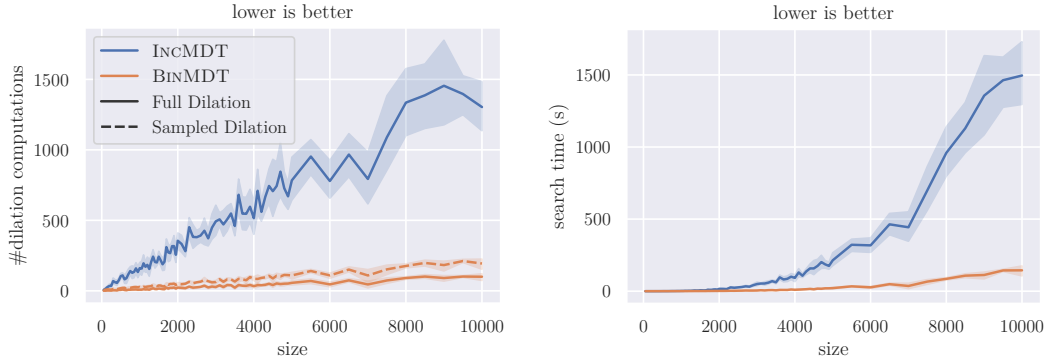
5.4 Q2: Initial solutions

Better initial solutions can reduce the number of candidate edges further than bad ones and thus affect the runtime of the overall algorithm. Delaunay triangulations are a natural choice for the initial solution, but we suspect that they can be improved by adding shortcut edges. Figure 7 shows that the relative dilation gap between the Delaunay triangulation and the optimal solution for the *random* instance set. It can be seen that the introduction of shortcut edges can indeed reduce the gap to the MDT to around 1.5%.

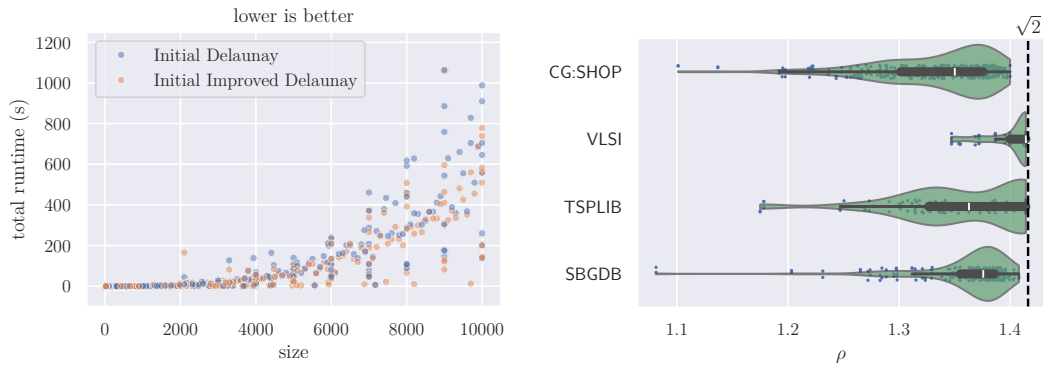
5.5 Q3: Comparison to state-of-the-art

We compare our approaches to two exact state-of-the-art algorithms for the MDT. Note that both of these use floating-point arithmetic and are not guaranteed to find the optimal solution. However, we can confirm that all previous solutions are within a small relative error of our optimal solution. The first approach is an integer programming (IP) approach by [8] that used the commercial software CPLEX to solve the MDT. The second comparison is with the most recent exact algorithm (BnB) from Sattari and Izadi [43]. For both approaches the source code is no longer available, so we cannot compare our results on the same hardware. Also for BnB [43] the instance data and results are no longer available. For both approaches we therefore use the data the authors published in their papers. Note that the drastic runtime difference that we see in our experiments cannot be attributed to improved hardware alone.

For *random-small*, both INCM and BIN outperform the IP and BnB approach by a large margin (up to four orders of magnitude), see Figure 7. All instances were solvable in less than 0.1s. Additionally, Sattari and Izadi [43] provided results for TSPLIB [42] instances (part of our *public* instance set) with up to 200 points. Table 1 shows that our approach is faster than the algorithm from Sattari and Izadi. We can solve instances to provable optimality in less than 1s while their algorithm took up to 1248s.



■ **Figure 8** Experiments on the *random* benchmark set. **(Left)** The number of dilation computations of BINMDT is significantly reduced compared to the incremental algorithm. **(Right)** BINMDT is significantly faster than the incremental algorithm.



■ **Figure 9** Experiments on the *public* benchmark set. **(Left)** Using the improved Delaunay triangulation as an initial solution significantly improved the performance. **(Right)** The dilation of the MDTs is at most $\sqrt{2}$ for all instances.

5.6 Q4: Algorithm comparison

We now compare INCMDT to BINMDT; see Appendix B.2 for more detail. Recall that BINMDT aims to reduce the time spent on dilation computations by reducing the number of dilation computations and merely sampling the dilation whenever that suffices. The first experiment was conducted on the *random* instances with up to 10,000 points; this experiment confirms that BINMDT indeed achieves a significantly lower runtime, requires fewer dilation computations, and that sampling is sufficient in most cases, see Figure 8.

After we confirmed that BINMDT is superior, we conducted an additional experiment with two different initial solution strategies on the *public* instances up to 10,000 points, see Figure 9. The first strategy uses the Delaunay triangulation as an initial solution; the second strategy uses the improved Delaunay triangulation with shortcut edges. The improved Delaunay triangulation significantly reduces the runtime of BINMDT for almost all instances. Detailed results for all instances of the *public* instance set are shown in Table 4. An additional experiment on the *public* instance set shows that BINMDT can solve instances with up to 30,000 points in less than 17h to provable optimality, see Table 3.

6 Improved bounds for regular n -gons

Vertex sets of regular n -gons are particularly challenging, as there are no points in the interior to serve as Steiner points for shortcuts, making local heuristics less successful. They are also natural candidates for worst-case dilation, as each diagonal constitutes an obstacle for the separated points. Thus, they have received considerable attention [37, 20, 45], with a lower bound of 1.4308 (see [20]) and an upper bound of 1.4482 (see [45]) on their worst-case dilation. Improving this gap is an open question posed by [20, Problem 1], originating from [7, 31]. With the help of our exact algorithm (see Appendix C), we were able to compute bounds for $n \in \{4, 5, \dots, 100\}$, answering the problem by Dumitrescu and Ghosh.

Our implementation currently uses floating-point precision to represent the coordinates of the input points. Thus, we cannot exactly represent the necessarily irrational points of any regular n -gon ($n \geq 5$) in our solver. However, we can compute the MDT of a rational point set that is a good approximation of a regular n -gon. We can then bound the error and thus obtain a rigorous lower bound on the dilation of the regular n -gon.

► **Theorem 6.** *Let P be a set of $n = 84$ points placed at the vertices of a regular n -gon. Then the dilation of the MDT of P is $\rho \geq 1.44116645381$.*

Proof. Let P be the point set of a regular 84-gon and Q be a point set that contains floating-point approximations of the points of P . There is a bijection $f : P \rightarrow Q$ with inverse f^{-1} that maps each point in P to the closest point in Q . For a given triangulation or path of P , we write $f(\cdot)$ to denote the triangulation or path where the points are transformed by pointwise application of f . Neither P nor Q contain collinear points and all points are in convex position, therefore T is a triangulation of P iff $f(T)$ is a triangulation of Q .

Let $\epsilon \geq \max_{p_i, p_j \in P} |d(p_i, p_j) - d(f(p_i), f(p_j))|$ be a bound on the maximum absolute error on distances and let δ be a chosen such that

$$\forall p_i, p_j \in P : (1 - \delta)d(p_i, p_j) \leq d(f(p_i), f(p_j)) \leq (1 + \delta)d(p_i, p_j).$$

Let T be the MDT of P with dilation ρ . Let $f(p_i), f(p_j)$ be a dilation-defining pair in $f(T)$ with path $\pi \subset Q$. Because T has dilation ρ , we have (i) $|f^{-1}(\pi)|/d(p_i, p_j) \leq \rho$. As π has at most $n - 1$ edges, we have (ii) $|\pi| - (n - 1)\epsilon \leq |f^{-1}(\pi)| \leq |\pi| + (n - 1)\epsilon$ and thus the following upper bound on the MDT of Q .

$$\begin{aligned} \frac{|\pi|}{d(f(p_i), f(p_j))} &= \frac{|\pi| - (n - 1)\epsilon}{d(f(p_i), f(p_j))} + \frac{(n - 1)\epsilon}{d(f(p_i), f(p_j))} \stackrel{(ii)}{\leq} \frac{|f^{-1}(\pi)|}{(1 - \delta)d(p_i, p_j)} + \frac{(n - 1)\epsilon}{d(f(p_i), f(p_j))} \\ &\stackrel{(i)}{\leq} \frac{1}{1 - \delta}\rho + \frac{(n - 1)\epsilon}{d(f(p_i), f(p_j))} \leq \frac{1}{1 - \delta}\rho + \frac{(n - 1)\epsilon}{\min_{q_i, q_j \in Q} d(q_i, q_j)}. \end{aligned}$$

Using exact calculations done with *sympy*, we computed $\epsilon \leq 2.730751 \cdot 10^{-16}$ and $\delta \leq 6.458762 \cdot 10^{-16}$, which, combined with the lower bound on the dilation of Q from our solver gives us $\rho \geq 1.44116645381$. ◀

7 Conclusion

We have presented exact algorithms for minimum dilation triangulations, greatly outperforming previous methods from the literature. This has also yielded insights into the intricate structure of optimal solutions for regular n -gons, together with new lower bounds on the

worst-case dilation of triangulations. This demonstrates the value of computational tools for gaining analytic insights that seem out of reach with purely manual analysis.

On the theoretical side, one tantalizing open question remains the complexity of the MDT; here the intricate structure of solutions for regular n -gons may show the way for hardness constructions even for convex arrangements. An equally fascinating problem is the worst-case dilation of triangulations; here we conjecture that the asymptotic dilation for regular n -gons corresponds to the worst-case dilation for general point sets, implying a value between 1.44116 and 1.4482, with a better lower bound achievable via even larger n -gons.

On the practical side, the runtime of our algorithms is dominated by repeatedly computing the dilation of a triangulation. With sums of square roots handled as described, this does not appear to be a difficult problem per se, so appropriately tailored algorithms or data structures for carrying out huge numbers of dilation queries would be extremely helpful.

References

- 1 Khaled M. Alzoubi, Xiang-Yang Li, Yu Wang, Peng-Jun Wan, and Ophir Frieder. Geometric spanners for wireless ad hoc networks. *IEEE Trans. Parallel Distributed Syst.*, 14(4):408–421, 2003. doi:10.1109/TPDS.2003.1195412.
- 2 Narayanasetty Amarnadh and Pinaki Mitra. Upper bound on dilation of triangulations of cyclic polygons. In *Computational Science and Its Applications - ICCSA 2006*, volume 3980 of *Lecture Notes in Computer Science*, pages 1–9. Springer, 2006. doi:10.1007/11751540_1.
- 3 Boris Aronov, Mark de Berg, Otfried Cheong, Joachim Gudmundsson, Herman J. Haverkort, Michiel H. M. Smid, and Antoine Vigneron. Sparse geometric graphs with small dilation. *Comput. Geom.*, 40(3):207–219, 2008. doi:10.1016/J.COMGEO.2007.07.004.
- 4 Marshall Bern and David Eppstein. Mesh generation and optimal triangulation. In *Computing in Euclidean geometry*, pages 47–123. World Scientific, 1995.
- 5 Ahmad Biniiaz, Mahdi Amani, Anil Maheshwari, Michiel H. M. Smid, Prosenjit Bose, and Jean-Lou De Carufel. A plane 1.88-spanner for points in convex position. *J. Comput. Geom.*, 7(1):520–539, 2016. doi:10.20382/JOCG.V7I1A21.
- 6 Johannes Blömer. Computing sums of radicals in polynomial time. In *Symposium on Foundations of Computer Science (FOCS)*, pages 670–677, 1991.
- 7 Prosenjit Bose and Michiel H. M. Smid. On plane geometric spanners: A survey and open problems. *Comput. Geom.*, 46(7):818–830, 2013. URL: <https://doi.org/10.1016/j.comgeo.2013.04.002>, doi:10.1016/J.COMGEO.2013.04.002.
- 8 Aléx F. Brandt, Miguel M. Gaiowski, Cid C. de Souza, and Pedro J. de Rezende. Minimum dilation triangulation: Reaching optimality efficiently. In *Proceedings of the 26th Canadian Conference on Computational Geometry, CCCG 2014, Halifax, Nova Scotia, Canada, 2014*. Carleton University, Ottawa, Canada, 2014. URL: <http://www.cccg.ca/proceedings/2014/papers/paper09.pdf>.
- 9 Kevin Buchin, Maike Buchin, Joachim Gudmundsson, and Sampson Wong. Bicriteria approximation for minimum dilation graph augmentation. In Timothy M. Chan, Johannes Fischer, John Iacono, and Grzegorz Herman, editors, *32nd Annual European Symposium on Algorithms, ESA 2024*, volume 308 of *LIPICs*, pages 36:1–36:15. Schloss Dagstuhl - Leibniz-Zentrum für Informatik, 2024. doi:10.4230/LIPICs.ESA.2024.36.
- 10 Leizhen Cai and Derek G. Corneil. Tree spanners. *SIAM J. Discret. Math.*, 8(3):359–387, 1995. doi:10.1137/S0895480192237403.
- 11 Barun Chandra, Gautam Das, Giri Narasimhan, and José Soares. New sparseness results on graph spanners. *Int. J. Comput. Geom. Appl.*, 5:125–144, 1995. doi:10.1142/S0218195995000088.
- 12 Otfried Cheong, Herman J. Haverkort, and Mira Lee. Computing a minimum-dilation spanning tree is NP-hard. *Comput. Geom.*, 41(3):188–205, 2008. doi:10.1016/J.COMGEO.2007.12.001.

- 13 Paul Chew. There is a planar graph almost as good as the complete graph. In *Proceedings of the Second Annual ACM SIGACT/SIGGRAPH Symposium on Computational Geometry*, pages 169–177. ACM, 1986. doi:10.1145/10515.10534.
- 14 Paul Chew. There are planar graphs almost as good as the complete graph. *J. Comput. Syst. Sci.*, 39(2):205–219, 1989. doi:10.1016/0022-0000(89)90044-5.
- 15 Mark de Berg, Otfried Cheong, Marc J. van Kreveld, and Mark H. Overmars. *Computational Geometry: Algorithms and Applications, 3rd Edition*. Springer, 2008. URL: <https://www.worldcat.org/oclc/227584184>.
- 16 Erik D Demaine, Sándor P Fekete, Phillip Keldenich, Dominik Krupke, and Joseph S. B. Mitchell. Computing convex partitions for point sets in the plane: The CG:SHOP Challenge 2020. *arXiv preprint arXiv:2004.04207*, 2020.
- 17 Erik D Demaine, Sándor P. Fekete, Phillip Keldenich, Dominik Krupke, and Joseph S. B. Mitchell. Area-optimal simple polygonalizations: The CG Challenge 2019. *Journal of Experimental Algorithmics (JEA)*, 27(2):1–12, 2022.
- 18 Erik D. Demaine, Joseph S. B. Mitchell, and Joseph O’Rourke. The open problems project: Problem #33, 2001. URL: <http://topp.openproblem.net/>.
- 19 Maria Gisela Dorzán, Mario Guillermo Leguizamón, Efrén Mezura-Montes, and Gregorio Hernández-Peñalver. Approximated algorithms for the minimum dilation triangulation problem. *J. Heuristics*, 20(2):189–209, 2014. doi:10.1007/S10732-014-9237-2.
- 20 Adrian Dumitrescu and Anirban Ghosh. Lower bounds on the dilation of plane spanners. *Int. J. Comput. Geom. Appl.*, 26(2):89–110, 2016. doi:10.1142/S0218195916500059.
- 21 Herbert Edelsbrunner and Tiow Seng Tan. A quadratic time algorithm for the minimax length triangulation. *SIAM J. Comput.*, 22(3):527–551, 1993. doi:10.1137/0222036.
- 22 Günther Eder, Martin Held, Steinþór Jasonarson, Philipp Mayer, and Peter Palfrader. Salzburg database of polygonal data: Polygons and their generators. *Data in Brief*, 31:105984, 2020. doi:10.1016/j.dib.2020.105984.
- 23 Friedrich Eisenbrand, Matthieu Haeberle, and Neta Singer. An improved bound on sums of square roots via the subspace theorem. In *Symposium on Computational Geometry (SoCG)*, 2024.
- 24 David Eppstein. Spanning trees and spanners. In Jörg-Rüdiger Sack and Jorge Urrutia, editors, *Handbook of Computational Geometry*, pages 425–461. North Holland / Elsevier, 2000. doi:10.1016/B978-044482537-7/50010-3.
- 25 Kai-Wei Fan, Sha Liu, and Prasun Sinha. Scalable data aggregation for dynamic events in sensor networks. In Andrew T. Campbell, Philippe Bonnet, and John S. Heidemann, editors, *Proceedings of the 4th International Conference on Embedded Networked Sensor Systems, SenSys 2006*, pages 181–194. ACM, 2006. doi:10.1145/1182807.1182826.
- 26 Arthur M. Farley, Andrzej Proskurowski, Daniel Zappala, and Kurt J. Windisch. Spanners and message distribution in networks. *Discret. Appl. Math.*, 137(2):159–171, 2004. doi:10.1016/S0166-218X(03)00259-2.
- 27 Sándor P. Fekete, Winfried Hellmann, Michael Hemmer, Arne Schmidt, and Julian Troegel. Computing maxmin edge length triangulations. *J. Comput. Geom.*, 9(1):1–26, 2018. doi:10.20382/JOCG.V9I1A1.
- 28 Laurent Fousse, Guillaume Hanrot, Vincent Lefèvre, Patrick Pélissier, and Paul Zimmermann. MPFR: A multiple-precision binary floating-point library with correct rounding. *ACM Trans. Math. Softw.*, 33(2):13, 2007. doi:10.1145/1236463.1236468.
- 29 Panos Giannopoulos, Rolf Klein, Christian Knauer, Martin Kutz, and Dániel Marx. Computing geometric minimum-dilation graphs is NP-hard. *Int. J. Comput. Geom. Appl.*, 20(2):147–173, 2010. doi:10.1142/S0218195910003244.
- 30 Andreas Haas. Solving large-scale minimum-weight triangulation instances to provable optimality. In *34th International Symposium on Computational Geometry, SoCG 2018*, volume 99 of *LIPICs*, pages 44:1–44:14. Schloss Dagstuhl - Leibniz-Zentrum für Informatik, 2018. doi:10.4230/LIPICs.SOCG.2018.44.

- 31 Iyad Kanj. Geometric spanners: Recent results and open directions. In *Third International Conference on Communications and Information Technology, ICCIT 2013*, pages 78–82. IEEE, 2013. doi:10.1109/ICCITECHNOLOGY.2013.6579526.
- 32 Alexander Klein. Effiziente Berechnung einer dilationsminimalen Triangulierung, 2006.
- 33 Christian Knauer and Wolfgang Mulzer. An exclusion region for minimum dilation triangulations. In *(Informal) Proceedings of the 21st European Workshop on Computational Geometry (EuroCG 2005)*, pages 33–36. Technische Universiteit Eindhoven, 2005. URL: <http://www.win.tue.nl/EWCG2005/Proceedings/9.pdf>.
- 34 László Kozma. Minimum average distance triangulations. In Leah Epstein and Paolo Ferragina, editors, *20th Annual European Symposium on Algorithms (ESA 2012)*, volume 7501 of *Lecture Notes in Computer Science*, pages 695–706. Springer, 2012. doi:10.1007/978-3-642-33090-2_60.
- 35 Joseph SB Mitchell and Wolfgang Mulzer. Proximity algorithms. In *Handbook of Discrete and Computational Geometry*, pages 849–874. CRC Press, Inc., 2017.
- 36 Bernard M. E. Moret and Henry D. Shapiro. *Algorithms from P to NP (vol. 1): Design and Efficiency*. Benjamin-Cummings Publishing Co., Inc., USA, 1991.
- 37 Wolfgang Mulzer. Minimum dilation triangulations for the regular n-gon. *Master's Thesis. Freie Universität Berlin, Germany.*, 2004.
- 38 Wolfgang Mulzer and Günter Rote. Minimum-weight triangulation is NP-hard. *J. ACM*, 55(2):11:1–11:29, 2008. doi:10.1145/1346330.1346336.
- 39 Giri Narasimhan and Michiel H. M. Smid. Approximating the stretch factor of euclidean graphs. *SIAM J. Comput.*, 30(3):978–989, 2000. doi:10.1137/S0097539799361671.
- 40 Giri Narasimhan and Michiel H. M. Smid. *Geometric spanner networks*. Cambridge University Press, 2007.
- 41 Joseph O'Rourke. Advanced problem 6369. *Amer. Math. Monthly*, 88(10):769, 1981.
- 42 G. Reinelt. TSPLIB—A Traveling Salesman Problem Library. *ORSA Journal of Computing*, 3(4):376–384, 1991.
- 43 Sattar Sattari and Mohammad Izadi. An exact algorithm for the minimum dilation triangulation problem. *J. Glob. Optim.*, 69(2):343–367, 2017. doi:10.1007/S10898-017-0517-X.
- 44 Sattar Sattari and Mohammad Izadi. Upper bounds for minimum dilation triangulation in two special cases. *Inf. Process. Lett.*, 133:33–38, 2018. doi:10.1016/J.IPL.2018.01.001.
- 45 Sattar Sattari and Mohammad Izadi. An improved upper bound on dilation of regular polygons. *Comput. Geom.*, 80:53–68, 2019. doi:10.1016/J.COMGEO.2019.01.009.
- 46 FNU Shariful, Justin Weathers, Anirban Ghosh, and Giri Narasimhan. Engineering an algorithm for constructing low-stretch geometric graphs with near-greedy average-degrees. *CoRR*, 2023. arXiv:2305.11312.
- 47 Israel Vite Silva, Nareli Cruz Cortés, Gregorio Toscano Pulido, and Luis Gerardo de la Fraga. Optimal triangulation in 3D computer vision using a multi-objective evolutionary algorithm. In *Applications of Evolutionary Computing, EvoWorkshops 2007*, volume 4448 of *Lecture Notes in Computer Science*, pages 330–339. Springer, 2007. doi:10.1007/978-3-540-71805-5_36.
- 48 Richard P Stanley. *Catalan numbers*. Cambridge University Press, 2015.
- 49 Victor J. D. Tsai. Delaunay triangulations in TIN creation: An overview and a linear-time algorithm. *Int. J. Geogr. Inf. Sci.*, 7(6):501–524, 1993. doi:10.1080/02693799308901979.
- 50 Chun-Hsien Wu, Kuo-Chuan Lee, and Yeh-Ching Chung. A delaunay triangulation based method for wireless sensor network deployment. *Comput. Commun.*, 30(14-15):2744–2752, 2007. doi:10.1016/J.COMCOM.2007.05.017.
- 51 Ge Xia. The stretch factor of the delaunay triangulation is less than 1.998. *SIAM J. Comput.*, 42(4):1620–1659, 2013. doi:10.1137/110832458.
- 52 Hongyu Zhou, Hongyi Wu, Su Xia, Miao Jin, and Ning Ding. A distributed triangulation algorithm for wireless sensor networks on 2d and 3d surface. In *30th IEEE International Conference on Computer Communications (INFOCOM 2011)*, pages 1053–1061. IEEE, 2011. doi:10.1109/INFCOM.2011.5934879.

A Implementation details

In this section, we describe relevant details omitted in the text above.

A.1 Enumeration process

Here we describe the implementation details omitted from Section 3.

A.1.1 Precise activation distances

Before resorting to the simplified activation distance computation described in Section 3.3, we attempted to compute precise upper bounds on the approximation distance using the elliptic arc and interval arithmetic as follows. We began by finding parameters a, b, c, d, e, f that describe the ellipse using the equation $ax^2 + bxy + cy^2 + dx + ey + f = 0$, based on 5 points on the ellipse; this involves solving a linear system with 6 variables and unknowns.

We then continued by a bisection search to find the maximum distance from p to the full ellipse on which the elliptic arc bounding the dead sector lies. In each iteration of this procedure, we have to check whether a circle with center p and some radius r intersects the ellipse, and if the intersection is possibly between the two rays that form the other bounds of the dead sector.

The intersection points of this circle with the ellipse are the roots of a quartic equation. Therefore, in each iteration, we have to check whether a quartic equation has a real root. We found that this computation is costly and numerically unstable; using interval arithmetic to compute a safe upper bound often produced overly conservative results. This was mostly due to strong amplification of minute uncertainties contained in a, \dots, f when evaluating the 6th-degree discriminant of the quartic equation to check for real roots; even in cases that were not deliberately constructed to be numerically challenging, we observed that the computation of the activation distance yielded results that were sometimes worse than what the much cheaper bounding rectangle-based approach gave us.

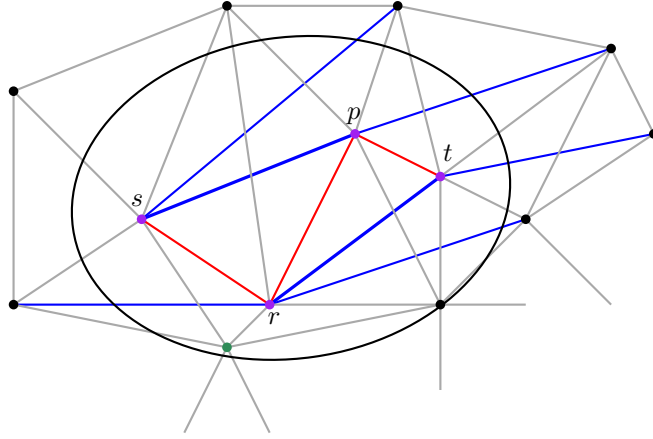
A.1.2 Dead sector construction

We now discuss which other points we use to construct dead sectors when we encounter a point t . During preliminary experiments, we found it insufficient to consider the closest points to t w.r.t. the polar angle around p . Points that are angularly near still can have high Euclidean distance, leading to a large activation distance or an empty dead sector. For efficiency reasons, it may also be costly to consider large sets, such as all previously encountered points. We only use a number that is $O(1)$ on average for each point t ; this is also needed to guarantee that the overall runtime of the algorithm is at most $O(n^2 \log n)$: otherwise, we might have significantly more dead sectors than points.

We use the following heuristics to determine *interesting neighbors* of a point t with which we attempt to construct dead sectors. Firstly, we do consider a small constant number of previously encountered points q that are close to t in terms of polar angle. Secondly, before running the actual enumeration process, we determine for each point a small number of interesting neighbors: aside from the six closest neighbors of t , we also consider all neighbors of t in the Delaunay triangulation.

A.2 Exact algorithm

In this section, we describe details omitted from Section 4.



■ **Figure 10** Sketch of the dilation path separation between s and t ; the red path represents the shortest s - t -path in the current triangulation T . The ellipse represents the points with total distance $\rho \cdot d(s, t)$ to s, t . Red and gray edges represent the current triangulation T and are a subset of E , blue edges are possible edges in E , but not in T . The green point is found from s but eliminated when running Dijkstra from t ; the purple points are the points in Q that may be on sufficiently short s - t -paths. The clause we generate contains the bold blue edges sp and rt ; without these edges, there is no sufficiently short s - t -path in E .

A.2.1 Dilation path separation in practice

Recall that solving the dilation path separation problem is a crucial part of our exact algorithm. We need to repeatedly and exactly compute shortest s - t -paths on our triangulation supergraph G to build a set of edges $E' \subseteq E \setminus T$ without which there is no sufficiently short s - t -path; we then return $\bigvee_{e \in E'} x_e$ as a clause that is violated by the current solution but satisfied by any solution with dilation less than ρ .

In order to speed up the computation, we begin by enumerating the vertices that may be on a sufficiently short s - t -path. We start by running a bounded version of Dijkstra's algorithm from s to enumerate the set Q of all vertices v that are reachable from s in distance less than $\rho \cdot d(s, t) - d(v, t)$. If this fails to reach t , we know that no sufficiently short path exists. In this case, we can immediately return the empty clause, which is always violated, as no solution with dilation less than ρ exists.

Otherwise, we further restrict Q by running a second bounded Dijkstra's algorithm from t , this time only considering vertices v reachable from t in distance less than $\rho \cdot d(s, t) - |\pi_G(s, v)|$, using the shortest path distances computed by the run from s .

We also restrict the set of possible edges by checking for each edge between two possible vertices $u, v \in Q$ whether either of the two paths $\pi_G(s, v), \pi_G(u, t)$ or $\pi_G(s, u), \pi_G(v, t)$ is shorter than $\rho \cdot d(s, t)$.

Afterwards, we can repeatedly run a bidirectional version of Dijkstra's algorithm, which simultaneously runs the algorithm from s and t , restricted to the possible vertices and edges to find a shortest path π between s and t ; after each run, if the path is shorter than $\rho \cdot d(s, t)$, we add an edge $e \notin T$ from π to E' , ignoring e in all subsequent bidirectional Dijkstra runs; see Figure 10 for an illustration. As soon as the shortest path exceeds $\rho \cdot d(s, t)$ or does not exist, we have found a suitable E' .

In practice, we have no efficient oracle for square root sum comparisons; see our remarks on computing exact shortest paths in Appendix A.3 for details on how we handle this.

A.2.2 Incremental SAT solving

Many modern SAT solvers are incremental, at least to some extent. Among other things, this means that we can add clauses to the solver after solving a formula and check whether the new set of clauses is satisfiable. This is often much more efficient than reconstructing the solver and re-solving the formula from scratch. Among other things, the solver gets to keep learned clauses and often also parts of the current state of the search; we see this reflected in the fact that, when we add clauses in INCMDT, the majority of the triangulation usually remains unchanged even though the solver could theoretically change large parts of the triangulation.

However, we must be more careful in BINMDT. As soon as we have used an incremental SAT solver on a bound that cannot be achieved, we have to construct a new solver object. This is because clauses may have been added to the solver that are not valid for less tight bounds. We therefore maintain a pool of clauses that we have generated; this allows us to quickly reconstruct a new SAT solver without losing such clauses. All clauses that we generate during the current iteration are only added to that pool once we have found a triangulation that satisfies the current bound.

We could alternatively generate tentative clauses by adding an *assumption literal* a_i on a new variable to all clauses generated by the i th iteration of BINMDT. We could then tell the incremental solver to temporarily *assume* that a_i is false, which would effectively enforce the clauses. If we find a triangulation satisfying the bound, we can make this assumption permanent by adding $\neg a_i$ as clause. If we instead find the bound to be too tight, we can disable the clauses by removing the assumption and adding a_i as clause.

We did not study this aspect further, since the time spent in the SAT solver was negligible compared to the time spent computing dilations.

A.3 Exactness

Ultimately, we aim for solutions that are exactly optimal, including all numerical issues, as if we were using infinite precision for all our computations. In this section, we describe the practical challenges this presents and our approach to handling them.

A.3.1 Dilation and shortest paths

Achieving this requires us to exactly compute the dilation. We thus rely on an exact implementation of Dijkstra's algorithm for Euclidean distances. We run Dijkstra's algorithm once for each source point p , computing the ratio between the shortest path and the Euclidean distance for p and all other points. The theoretical runtime for this is $O(n^2 \log n)$ assuming uniform cost for each computational operation; we parallelize the runs for different source points. We represent each dilation value as a combination of a path defining the dilation and an interval containing the true dilation value. In most cases, interval arithmetic is sufficient to decide which path defines the dilation; however, in particular in some non-randomly generated instances that include symmetries, we encounter cases where intervals do not suffice. In fact, the path defining the dilation is often non-unique in these instances.

In a first prototype, we simply resorted to directly constructing an instance of CGAL's exact number type with support for square roots, representing the precise dilation values in order to compare them if interval arithmetic was insufficient. However, the comparisons resulted in unacceptable performance issues; it turned out to be crucial to perform extensive preprocessing before resorting to such expensive operations: even single comparisons of sums consisting of less than 10 square roots each often took several seconds or minutes.

Let $\pi_1 = (p_1, \dots, p_k)$ and $\pi_2 = (q_1, \dots, q_m)$ be two paths for which we want to decide which one incurs a worse detour. In other words, we want to determine whether

$$\frac{\sum_{i=2}^k d(p_{i-1}, p_i)}{d(p_1, p_k)} = \underbrace{\sum_{i=2}^k \frac{d(p_{i-1}, p_i)}{d(p_1, p_k)}}_{(*)} \stackrel{?}{<} \frac{\sum_{i=2}^m d(q_{i-1}, q_i)}{d(q_1, q_m)} = \underbrace{\sum_{i=2}^m \frac{d(q_{i-1}, q_i)}{d(q_1, q_m)}}_{(**)}.$$

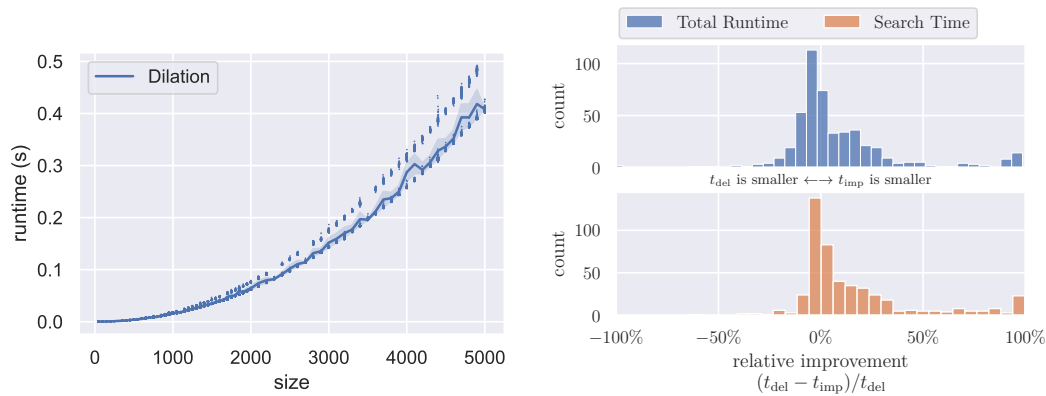
Observe that each entry of the sums $(*)$ and $(**)$ is the square root of a rational number; we can compute and compare these rational numbers at much lower cost than dealing with the square roots. This allows us to eliminate equal terms from the sums $(*)$ and $(**)$. We also scan for horizontal or vertical segments, which have rational length for rational input coordinates, and collect them in a single term on each side.

We use these rational numbers to compute more precise intervals for each of the terms, summing up $(*) - (**)$ in interval arithmetic in order of increasing absolute value. If the resulting interval does not contain 0, we can decide which path has higher dilation. If it is precisely $[0, 0]$, e.g., because we eliminated all terms, we know both paths have the same dilation. Otherwise, we repeat the computation using intervals of 1024-bit mantissa floating point values using the MPFR [28] library instead of double-precision values. Only if all these steps fail do we construct the dilation values using CGAL's exact number type and compare them; in all cases we observed, at this point, the resulting values were actually equal. We apply similar techniques to compare the length of paths instead of dilations in our implementation of Dijkstra's algorithm.

A.3.2 Candidate edge enumeration

Not only the computation of shortest paths and the dilation require attention to numerical issues, but these are the only cases necessarily involving the comparison of sums of square roots. The incremental search procedure is also exact, i.e., events regarding points and nodes are handled in precisely the correct order, while activation distance events are handled based on upper bounds on the exact activation distance. We order all events by squared distances instead of distances and thus maintain rationality, allowing us to augment interval arithmetic with rational computations to ultimately decide the order of events. Most other parts of the enumeration process only require exact predicates, such as intersections checks; these are provided by CGAL and also make use of interval arithmetic to only resort to exact computations if necessary.

Another situation where the use of interval arithmetic is important and not straightforward is the representation of dead sectors. Since working with true polar angles involves the costly trigonometric function `atan2`, which is not readily available with correct rounding for use in interval arithmetic, we instead use *pseudo-angles* as described by Moret and Shapiro [36]. In essence, we measure angles by computing distances along the ℓ_1 unit circle instead of the ℓ_2 unit circle. Pseudo-angles are rational and only use operations that are available in correctly-rounded fashion on modern CPUs; this allows us to use interval arithmetic to handle the polar angle intervals of dead sectors. In order to allow us to merge polar angle intervals that touch in a single point, which would not be possible using interval arithmetic alone, we also store, for each polar angle interval, the lowest and highest point (w.r.t. the pseudo-angle around p) in the interval.



■ **Figure 11 (Left)** The dilation computation time increases significantly for larger instances. **(Right)** Runtime impact of working with the Delaunay triangulation (t_{del}) directly vs. using the initial improvement algorithm (t_{imp}). Introducing initial improvements reduces the search time of BINMDT significantly but can come at the cost of a higher overall runtime.

B Empirical evaluation

In this section, we provide additional details on the experiments conducted in the context of the empirical evaluation, together with additional figures and data tables; note that all experiment data are archived and publicly accessible; see the supplement.

QA1 How does the runtime of the dilation computation scale with the number of points in the input instance?

B.1 QA1: Dilation computation

The proposed algorithms rely on the computation of the dilation for some given triangulation. Our implementation uses an exact version of a bidirectional Dijkstra algorithm to compute the dilation in $O(n^2 \log n)$, see Appendix A.3 for details. The experiment was conducted on the *random* instance set with up to 5000 points where the input triangulation is the Delaunay triangulation. To obtain a reasonable average runtime, we computed the dilation for each instance 100 times, see Figure 11. A dilation query for an instance with 5000 points takes on average slightly more than 0.4s. As expected, the runtime increases with the number of points in the instance with a quadratic dependency. In our experiments on the *public* instance set we observed that the runtime of the dilation computation can be significantly higher. This is due to degenerate instances containing structures like regular grids that have a lot of edges and paths with the same length. Doing exact comparisons of square roots in these cases can be costly and lead to higher runtimes.

B.2 Q4: Algorithm comparison

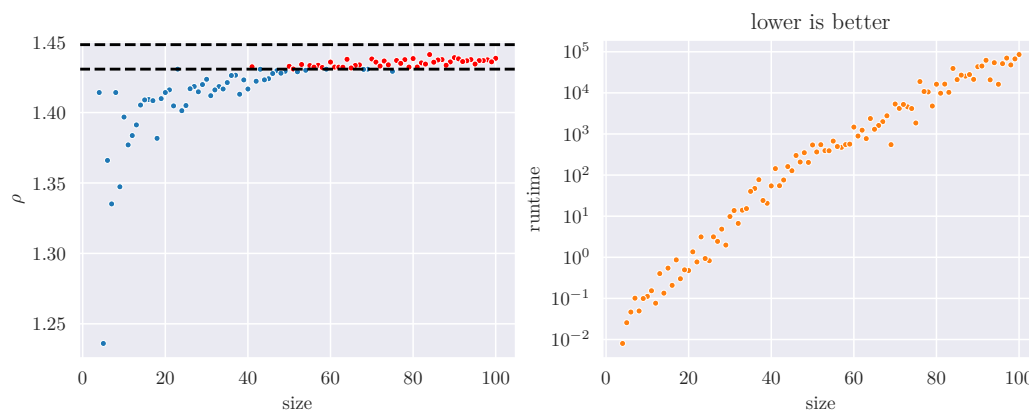
This section contains additional details on the comparison of the proposed algorithms to each other and should be seen as an extension to Section 5.6. Figure 9 shows the runtime of the BINMDT with two different initial solution strategies on the *public* benchmark set with up to 10,000 points.

We provide an additional information in Figure 11 that shows the relative runtime change when using the different initial solution strategies. Let t_{del} be the runtime of BINMDT when

instance	ρ	BnB [43] runtime (s)	BINMDT runtime (s)
burma14	1.1749	0.0040	0.0061
ulysses16	1.1782	0.0060	0.0010
ulysses22	1.1782	0.0230	0.0077
att48	1.3279	0.6570	0.0098
eil51	1.3306	0.6990	0.0070
berlin52	1.2693	1.4140	0.0097
st70	1.3002	8.5910	0.0099
eil76	1.3407	4.3370	0.0018
pr76	1.3013	26.7950	0.0340
gr96	1.3310	20.4990	0.0031
rat99	1.3280	31.1510	0.0133
kroA100	1.3386	18.3480	0.0027
kroB100	1.2910	18.4390	0.0097
kroC100	1.3263	17.6490	0.0215
kroD100	1.3159	19.3270	0.0153
kroE100	1.3416	21.0360	0.0270
rd100	1.3328	18.7420	0.0180
eil101	1.4142	14.8230	0.0153
lin105	1.3116	36.7820	0.0217
pr107	1.2504	55.8490	0.1261
pr124	1.3077	67.2010	0.0305
bier127	1.2999	47.7660	0.0231
ch130	1.3535	61.8330	0.0549
pr136	1.4037	159.0230	0.0066
gr137	1.2732	126.4090	0.0146
pr144	1.2469	1248.7270	0.2512
ch150	1.3032	112.2890	0.0195
kroA150	1.3386	107.5780	0.0038
kroB150	1.3217	113.8820	0.0169
pr152	1.2770	547.4960	0.2999
u159	1.4142	158.4300	0.0501
rat195	1.3436	610.1950	0.0274
d198	1.4142	1131.8730	0.0124
kroA200	1.3863	397.6640	0.0572
kroB200	1.3804	398.1610	0.0055

■ **Table 1** Solutions and runtimes for small TSPLIB instances.

starting with the Delaunay triangulation as initial solution and t_{imp} be the runtime when starting with the improvement Delaunay triangulation. We distinguish between the overall runtime (including calculating the initial solution) and the search time (the time spent in finding the optimal solution). What we compare is the relative improvement, i.e. $\frac{t_{\text{del}} - t_{\text{imp}}}{t_{\text{del}}}$. A positive value indicates that the improved Delaunay triangulation reduces the runtime and a negative value indicates that the initial improvement increases the runtime. Regarding the search time we observe that the improved solution reduces the time it takes to find and verify the optimal solution. This is expected as the heuristic is known to produce better solutions than the Delaunay triangulation and in fact can never be worse than the Delaunay



■ **Figure 12** Dilations and runtimes for regular n -gons for $4 \leq n \leq 100$. Red dots improve the current lower bound on the dilation of regular n -gons of 1.4308 that comes from the regular 23-gon. The dashed black lines mark the known upper bound of 1.4482 and the previous best lower bound of 1.4308.

triangulation, see Section 5.4. The overall runtime however can sometimes be higher when using the improved triangulation as the initial solution. This is due to the fact that testing different constrained Delaunay triangulations require multiple dilation computations which can be costly. Still we conclude that using the improved initial solution is beneficial in most cases and is used as the default setting for the BINMDT algorithm.

C Additional remarks on regular n -gons

It was already noted by Euler (see [48]) that the number of triangulations of convex n -gons corresponds to the Catalan numbers C_{n-2} , which grow asymptotically like $\frac{4^n}{n^{3/2}\sqrt{\pi}}$, illustrating the futility of performing a brute-force enumeration for finding an MDT.

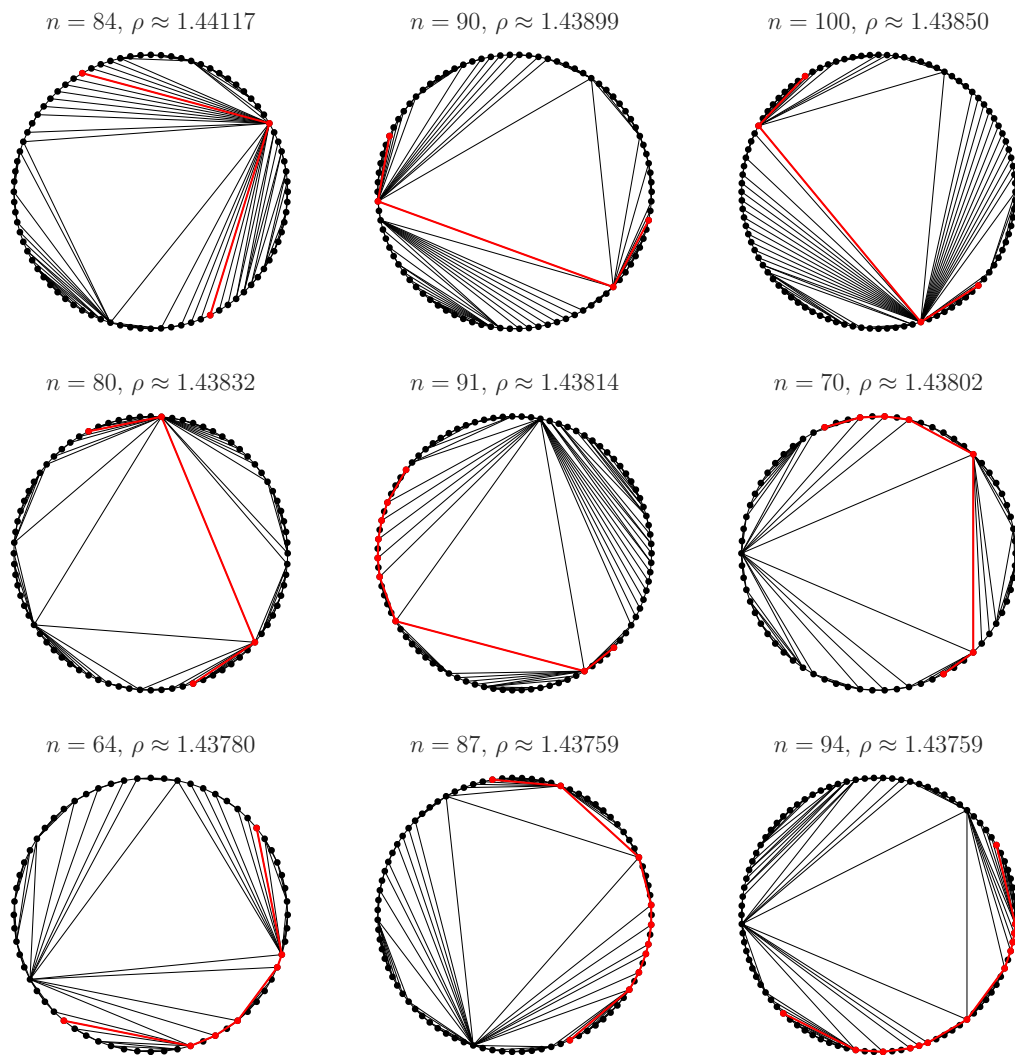
In Section 6 we answer the open question posed by Dumitrescu and Ghosh [20, Problem 1] that originated from Bose, Smit and Kanj [7, 31]. With the help of our exact algorithm we can obtain a lower bound for the dilation of regular n -gons. It is known that the worst-case dilation of a regular n -gon is between 1.4308 and 1.4482.

► **Theorem 7** ([20, 45]). *The worst-case dilation of a regular n -gon ρ^* is bounded by*

$$1.4308 \approx \frac{2 \sin(\frac{2\pi}{23}) + \sin(\frac{8\pi}{23})}{\sin(\frac{11\pi}{23})} \leq \rho^* < 1.4482.$$

We ran our exact algorithm for regular n -gons for $4 \leq n \leq 100$. Figure 12 highlights the previous bounds from Theorem 7 and shows that many regular n -gons improve the current lower bound of 1.4308. Figure 13 shows some examples of such solutions. One can observe that the solution structures appear to be quite intricate, highlighting that it would have been quite challenging to establish these results with only the help of manual analysis. Moreover, this intricacy may be an indication that the underlying problem does not lend itself to a simple polynomial-time algorithm.

These difficulties are also visible in the necessary runtimes for n -gons. It is remarkable that the growth (which appears to be exponential in n) is significantly faster than for our results on instances from the *uniform* and *public* benchmark sets (see Section 5.6), with already more than 10h for $n = 84$ points. (See Figure 12 and Table 2 for detailed results.)



■ **Figure 13** Optimal MDT of regular n -gon with floating point coordinates. All solutions improve the current lower bound for regular n -gons.

An intuitive reason may be that any point in the interior can be used as a Steiner point for shortcuts, while also allowing local reduction techniques such as the ellipse property, which fails to provide a reduction for the vertices of a regular n -gon. Conversely, any chord through the interior constitutes an obstacle for all separated point pairs, producing cascading sets of constraints. Moreover, any solution contains many symmetries that make finding an optimal solution (among many others with similar or same dilation) significantly harder. As all points are on the boundary of a circle, quadtree queries in the enumeration algorithm are not as effective as in other instance sets. Finally, regular n -gons contain a maximum number of intersections between edges, which makes intersection constraints weaker. It is this combination of difficulties that make regular n -gons all the more interesting, as they are prime candidates for the worst-case dilation bound.

► **Conjecture 8.** *The worst-case bound for Minimum Dilation Triangulations corresponds to the asymptotic value for regular n -gons. This implies that the correct value is 1.44...*

n	ρ	runtime (s)	n	ρ	runtime (s)	n	ρ	runtime (s)
4	1.41421	< 1	37	1.42651	77	70	1.43802	5357
5	1.23606	< 1	38	1.41300	24	71	1.43579	4190
6	1.36602	< 1	39	1.42316	21	72	1.43298	5236
7	1.33512	< 1	40	1.41671	55	73	1.43659	4574
8	1.41421	< 1	41	1.43250	144	74	1.43388	4160
9	1.34729	< 1	42	1.42222	55	75	1.42925	1850
10	1.39680	< 1	43	1.43074	76	76	1.43695	18,849
11	1.37703	< 1	44	1.42320	161	77	1.43490	10,805
12	1.38366	< 1	45	1.42403	128	78	1.43755	10,536
13	1.39121	< 1	46	1.42771	300	79	1.43228	4788
14	1.40532	< 1	47	1.42969	208	80	1.43832	16,235
15	1.40897	< 1	48	1.42791	350	81	1.43232	9818
16	1.40924	< 1	49	1.42927	203	82	1.43525	16,369
17	1.40844	< 1	50	1.43283	541	83	1.43441	10,314
18	1.38169	< 1	51	1.43089	365	84	1.44116	39,277
19	1.40988	< 1	52	1.42892	549	85	1.43574	21,030
20	1.41421	< 1	53	1.43411	393	86	1.43731	27,062
21	1.41610	1	54	1.42999	391	87	1.43759	25,565
22	1.40471	< 1	55	1.43335	672	88	1.43357	27,903
23	1.43081	3	56	1.43224	495	89	1.43592	21,326
24	1.40133	< 1	57	1.43356	474	90	1.43898	43,300
25	1.40497	< 1	58	1.43199	551	91	1.43814	45,019
26	1.41690	3	59	1.43077	567	92	1.43620	62,126
27	1.41850	2	60	1.43582	1472	93	1.43675	20,787
28	1.41472	5	61	1.43230	890	94	1.43758	54,273
29	1.41986	2	62	1.43221	1237	95	1.43442	16,205
30	1.42362	10	63	1.43217	772	96	1.43687	51,445
31	1.41196	14	64	1.43779	2376	97	1.43687	70,321
32	1.41607	7	65	1.43164	1302	98	1.43743	47,885
33	1.41845	14	66	1.43343	1609	99	1.43599	67,183
34	1.41671	15	67	1.43381	1995	100	1.43849	85,588
35	1.42127	40	68	1.43063	2773			
36	1.42630	47	69	1.43078	550			

■ **Table 2** Dilations of regular n -gons for $4 \leq n \leq 100$ and the runtime of the BINMDT algorithm. Bold values improve the current lower bound on the dilation of regular n -gons of 1.4308 that arises from the regular 23-gon.

D Additional tables

Here we provide a full overview of additional experiment data in table form.

instance	n	ρ	#full dil.	#sampled dil.	BINMDT time (s)
xmc10150	10150	1.4142	1	22	6
rl11849	11849	1.4142	1	10	4
usa13509	13509	1.3882	307	451	735
xvb13584	13584	1.4142	1	87	37
brd14051	14051	1.4142	1	21	6
xrb14233	14233	1.4142	1	15	5
d15112	15112	1.3852	105	199	332
xia16928	16928	1.4142	1	21	9
pjh17845	17845	1.4142	1	18	8
d18512	18512	1.4142	86	200	502
frh19289	19289	1.4142	1	91	59
fnc19402	19402	1.4142	1	8	4
pntset-0020000	20000	1.4018	229	434	1327
fpg-poly-0000020000	20000	1.3825	975	1208	4664
us-night-0020000	20000	1.3948	821	1037	4098
protein-0020000	20000	1.3949	780	1052	3952
uniform-0020000-2	20000	1.3861	291	508	1548
euro-night-0020000	20000	1.3936	971	1250	4990
uniform-0020000-1	20000	1.3903	290	537	1654
jupiter-0020000	20000	1.3829	3422	3934	16,384
ido21215	21215	1.4142	1	14	7
fma21553	21553	1.4142	1	62	61
lsb22777	22777	1.4142	1	41	29
xrh24104	24104	1.4142	1	78	78
bbz25234	25234	1.4142	1	26	17
irx28268	28268	1.4142	1	39	26
fyg28534	28534	1.4142	1	38	34
icx28698	28698	1.4142	1675	2026	32,372
boa28924	28924	1.4142	1	32	25
ird29514	29514	1.4142	1	45	52
protein-0030000	30000	1.3931	1798	2168	19,527
us-night-0030000	30000	1.3968	1683	1972	18,160
euro-night-0030000	30000	1.3976	1204	1506	13,871
uniform-0030000-1	30000	1.3946	322	615	4076
pntset-0030000	30000	1.3929	423	820	5635
fpg-poly-0000030000	30000	1.3885	1042	1341	11,842
uniform-0030000-2	30000	1.3870	414	779	5391
jupiter-0030000	30000	1.3785	3394	6129	58,752

Table 3 Solutions and runtimes of BINMDT for large instances of the *public* benchmark set. Columns also provide the number of full and sampled dilation computations that are the bottleneck in the exact algorithm.

instance	n	ρ	#full dil.	#sampled dil.	BINMDT time (s)
london-0000010	10	1.1010	1	7	< 1
stars-0000010	10	1.1953	1	5	< 1
pntset-0000010	10	1.2032	1	7	< 1
euro-night-0000010	10	1.2184	2	2	< 1
uniform-0000010-1	10	1.2528	2	4	< 1
fpg-poly-0000000010	10	1.0811	1	6	< 1
uniform-0000010-2	10	1.2215	1	9	< 1
us-night-0000010	10	1.1920	1	1	< 1
burma14	14	1.1749	1	8	< 1
stars-0000015	15	1.1368	1	5	< 1
london-0000015	15	1.2564	1	8	< 1
uniform-0000015-2	15	1.2225	1	7	< 1
uniform-0000015-1	15	1.2434	1	7	< 1
euro-night-0000015	15	1.1975	1	1	< 1
us-night-0000015	15	1.2868	2	8	< 1
ulysses16	16	1.1782	1	1	< 1
uniform-0000020-1	20	1.2368	1	8	< 1
uniform-0000020-2	20	1.3345	1	8	< 1
fpg-poly-0000000020	20	1.3152	1	8	< 1
pntset-0000020	20	1.2739	1	8	< 1
us-night-0000020	20	1.3101	1	7	< 1
euro-night-0000020	20	1.2824	1	8	< 1
london-0000020	20	1.2747	1	8	< 1
stars-0000020	20	1.1946	1	6	< 1
ulysses22	22	1.1782	1	7	< 1
euro-night-0000025	25	1.2483	1	7	< 1
uniform-0000025-1	25	1.2888	1	1	< 1
stars-0000025	25	1.2193	1	6	< 1
us-night-0000025	25	1.3488	1	9	< 1
uniform-0000025-2	25	1.3500	1	8	< 1
london-0000025	25	1.2960	2	6	< 1
london-0000030	30	1.3355	1	1	< 1
pntset-0000030	30	1.2720	2	7	< 1
fpg-poly-0000000030	30	1.2313	2	7	< 1
euro-night-0000030	30	1.2627	1	1	< 1
us-night-0000030	30	1.2997	2	3	< 1
uniform-0000030-2	30	1.3112	2	10	< 1
uniform-0000030-1	30	1.2722	1	7	< 1
stars-0000030	30	1.2653	1	1	< 1
us-night-0000035	35	1.2630	1	11	< 1
stars-0000035	35	1.3488	2	9	< 1
uniform-0000035-2	35	1.2930	1	8	< 1
uniform-0000035-1	35	1.2591	3	9	< 1
london-0000035	35	1.2363	1	6	< 1
euro-night-0000035	35	1.3131	1	1	< 1
stars-0000040	40	1.2998	1	5	< 1
london-0000040	40	1.2877	2	5	< 1

instance	n	ρ	#full dil.	#sampled dil.	BINMDT time (s)
pntset-0000040	40	1.2885	1	7	< 1
us-night-0000040	40	1.2897	1	6	< 1
euro-night-0000040	40	1.3022	1	1	< 1
fpg-poly-0000000040	40	1.2953	1	7	< 1
uniform-0000040-2	40	1.2608	3	8	< 1
uniform-0000040-1	40	1.3211	1	7	< 1
uniform-0000045-1	45	1.3216	2	7	< 1
us-night-0000045	45	1.2954	1	1	< 1
uniform-0000045-2	45	1.2830	2	5	< 1
london-0000045	45	1.2705	1	5	< 1
stars-0000045	45	1.2834	2	7	< 1
euro-night-0000045	45	1.2839	2	4	< 1
att48	48	1.3279	1	8	< 1
london-0000050	50	1.2953	1	7	< 1
uniform-0000050-2	50	1.3042	1	5	< 1
stars-0000050	50	1.3652	1	8	< 1
fpg-poly-0000000050	50	1.3485	1	8	< 1
uniform-0000050-1	50	1.2665	1	1	< 1
pntset-0000050	50	1.2845	3	7	< 1
euro-night-0000050	50	1.2926	3	10	< 1
us-night-0000050	50	1.2728	1	1	< 1
eil51	51	1.3306	1	6	< 1
berlin52	52	1.2693	3	8	< 1
fpg-poly-0000000060	60	1.2829	1	8	< 1
london-0000060	60	1.3246	2	9	< 1
us-night-0000060	60	1.2564	1	8	< 1
stars-0000060	60	1.3449	1	8	< 1
uniform-0000060-2	60	1.3171	3	5	< 1
pntset-0000060	60	1.3117	1	6	< 1
uniform-0000060-1	60	1.3149	1	6	< 1
euro-night-0000060	60	1.2973	1	7	< 1
uniform-0000070-2	70	1.2880	1	1	< 1
st70	70	1.3002	2	6	< 1
stars-0000070	70	1.3375	5	16	< 1
london-0000070	70	1.2838	4	11	< 1
euro-night-0000070	70	1.3233	3	9	< 1
fpg-poly-0000000070	70	1.2979	1	7	< 1
pntset-0000070	70	1.3298	1	8	< 1
uniform-0000070-1	70	1.2803	4	7	< 1
us-night-0000070	70	1.2949	2	10	< 1
pr76	76	1.3013	3	18	< 1
eil76	76	1.3407	1	1	< 1
pntset-0000080	80	1.2983	1	6	< 1
us-night-0000080	80	1.3090	1	6	< 1
uniform-0000080-1	80	1.3169	4	9	< 1
london-0000080	80	1.3399	3	9	< 1
stars-0000080	80	1.3066	3	10	< 1

instance	n	ρ	#full dil.	#sampled dil.	BINMDT time (s)
fpg-poly-000000080	80	1.3236	3	5	< 1
euro-night-0000080	80	1.3598	3	9	< 1
uniform-0000080-2	80	1.3059	1	6	< 1
uniform-0000090-1	90	1.3033	2	9	< 1
euro-night-0000090	90	1.3374	1	7	< 1
uniform-0000090-2	90	1.3021	3	10	< 1
stars-0000090	90	1.2900	1	5	< 1
fpg-poly-000000090	90	1.3479	3	12	< 1
us-night-0000090	90	1.3481	4	12	< 1
pntset-0000090	90	1.2975	3	4	< 1
london-0000090	90	1.3206	4	9	< 1
gr96	96	1.3310	1	1	< 1
rat99	99	1.3280	4	10	< 1
fpg-poly-000000100	100	1.2652	5	13	< 1
kroD100	100	1.3159	1	6	< 1
rd100	100	1.3328	2	10	< 1
kroE100	100	1.3416	2	13	< 1
kroA100	100	1.3386	1	1	< 1
stars-0000100	100	1.3448	1	16	< 1
us-night-0000100	100	1.3176	5	10	< 1
uniform-0000100-1	100	1.3335	1	1	< 1
london-0000100	100	1.3387	3	6	< 1
pntset-0000100	100	1.3420	1	12	< 1
uniform-0000100-2	100	1.3701	1	6	< 1
euro-night-0000100	100	1.3067	4	10	< 1
kroC100	100	1.3263	1	7	< 1
kroB100	100	1.2910	3	7	< 1
eil101	101	1.4142	1	8	< 1
lin105	105	1.3116	6	15	< 1
pr107	107	1.2504	41	45	< 1
pr124	124	1.3077	5	12	< 1
bier127	127	1.2999	3	9	< 1
ch130	130	1.3535	1	24	< 1
xqf131	131	1.3720	3	7	< 1
pr136	136	1.4037	1	2	< 1
gr137	137	1.2732	3	8	< 1
pr144	144	1.2469	40	67	< 1
kroA150	150	1.3386	1	1	< 1
kroB150	150	1.3217	3	9	< 1
ch150	150	1.3032	6	12	< 1
pr152	152	1.2770	71	141	< 1
u159	159	1.4142	1	8	< 1
rat195	195	1.3436	2	10	< 1
d198	198	1.4142	1	1	< 1
stars-0000200	200	1.3574	2	8	< 1
uniform-0000200-1	200	1.3563	2	9	< 1
paris-0000200	200	1.3278	5	11	< 1

instance	n	ρ	#full dil.	#sampled dil.	BINMDT time (s)
us-night-0000200	200	1.3354	5	16	< 1
kroB200	200	1.3804	1	1	< 1
fpg-poly-0000000200	200	1.3144	7	13	< 1
pntset-0000200	200	1.3582	1	6	< 1
uniform-0000200-2	200	1.3560	1	12	< 1
kroA200	200	1.3863	1	10	< 1
euro-night-0000200	200	1.3147	5	14	< 1
gr202	202	1.3184	2	7	< 1
ts225	225	1.4142	1	10	< 1
tsp225	225	1.4140	1	5	< 1
pr226	226	1.4142	1	8	< 1
gr229	229	1.3382	9	18	< 1
xqg237	237	1.3720	8	21	< 1
gil262	262	1.3209	6	14	< 1
pr264	264	1.3868	16	38	< 1
a280	279	1.4142	1	5	< 1
pr299	299	1.4142	1	3	< 1
stars-0000300	300	1.3392	18	34	< 1
uniform-0000300-2	300	1.3632	6	12	< 1
uniform-0000300-1	300	1.3317	6	15	< 1
us-night-0000300	300	1.3521	1	7	< 1
fpg-poly-0000000300	300	1.3500	4	19	< 1
pntset-0000300	300	1.3210	5	12	< 1
paris-0000300	300	1.3577	2	13	< 1
euro-night-0000300	300	1.3319	25	34	< 1
linhp318	318	1.3145	22	37	< 1
lin318	318	1.3145	22	37	< 1
pma343	343	1.3473	8	25	< 1
pka379	379	1.3473	5	26	< 1
bcl380	380	1.3720	15	28	< 1
pbl395	395	1.3473	6	21	< 1
euro-night-0000400	400	1.3486	23	32	< 1
stars-0000400	400	1.3601	7	18	< 1
uniform-0000400-2	400	1.3793	1	7	< 1
rd400	400	1.3489	10	21	< 1
fpg-poly-0000000400	400	1.3292	26	39	< 1
pntset-0000400	400	1.3443	5	11	< 1
us-night-0000400	400	1.3489	11	27	< 1
paris-0000400	400	1.3392	4	15	< 1
uniform-0000400-1	400	1.3762	1	7	< 1
pbk411	411	1.4123	6	18	< 1
fl417	417	1.4142	1	1	< 1
pbn423	423	1.3868	15	30	< 1
gr431	431	1.3409	7	16	< 1
pbn436	436	1.3868	12	24	< 1
pr439	439	1.4142	18	29	< 1
pcb442	442	1.4142	1	7	< 1

instance	n	ρ	#full dil.	#sampled dil.	BINMDT time (s)
d493	493	1.3416	9	17	< 1
us-night-0000500	500	1.3324	17	35	< 1
uniform-0000500-1	500	1.3420	9	20	< 1
pntset-0000500	500	1.3640	4	26	< 1
paris-0000500	500	1.3574	12	27	< 1
stars-0000500	500	1.3405	6	15	< 1
fpg-poly-0000000500	500	1.3463	1	1	< 1
euro-night-0000500	500	1.3611	16	28	< 1
uniform-0000500-2	500	1.3690	4	13	< 1
ali535	506	1.3361	27	46	< 1
att532	532	1.3630	4	12	< 1
u574	574	1.3814	4	18	< 1
rat575	575	1.3558	6	19	< 1
euro-night-0000600	600	1.3716	31	50	< 1
uniform-0000600-1	600	1.3625	3	7	< 1
paris-0000600	600	1.3797	1	1	< 1
pntset-0000600	600	1.3385	8	19	< 1
us-night-0000600	600	1.3999	1	20	< 1
stars-0000600	600	1.3642	11	31	< 1
uniform-0000600-2	600	1.3555	10	28	< 1
fpg-poly-0000000600	600	1.3541	27	36	< 1
p654	654	1.4142	1	8	1
d657	657	1.3473	28	43	< 1
xql662	662	1.3552	37	58	< 1
gr666	666	1.3409	16	27	< 1
stars-0000700	700	1.3536	15	28	< 1
uniform-0000700-2	700	1.3792	1	4	< 1
euro-night-0000700	700	1.3790	1	3	< 1
fpg-poly-0000000700	700	1.3664	12	37	< 1
uniform-0000700-1	700	1.3838	1	12	< 1
us-night-0000700	700	1.3763	10	30	< 1
pntset-0000700	700	1.3510	7	17	< 1
paris-0000700	700	1.3303	17	30	< 1
rbx711	711	1.4000	9	29	< 1
u724	724	1.4142	1	1	< 1
rbu737	737	1.4142	1	8	< 1
rat783	783	1.3613	5	17	< 1
stars-0000800	800	1.3572	11	22	< 1
euro-night-0000800	800	1.3425	44	63	< 1
uniform-0000800-2	800	1.3866	1	5	< 1
fpg-poly-0000000800	800	1.3795	25	44	< 1
pntset-0000800	800	1.3942	1	4	< 1
uniform-0000800-1	800	1.3701	13	28	< 1
paris-0000800	800	1.3504	1	8	< 1
us-night-0000800	800	1.3543	20	33	< 1
dkg813	813	1.4000	25	39	< 1
us-night-0000900	900	1.3611	38	71	< 1

instance	n	ρ	#full dil.	#sampled dil.	BINMDT time (s)
uniform-0000900-1	900	1.3636	5	17	< 1
euro-night-0000900	900	1.3655	52	70	< 1
stars-0000900	900	1.3352	28	44	< 1
uniform-0000900-2	900	1.3625	4	14	< 1
paris-0000900	900	1.3599	19	38	< 1
fpg-poly-0000000900	900	1.3551	38	51	< 1
pntset-0000900	900	1.3897	1	7	< 1
lim963	963	1.4142	1	5	< 1
pbd984	984	1.4142	1	5	< 1
skylake-0001000	1000	1.3660	12	26	< 1
dsj1000	1000	1.3471	49	66	< 1
us-night-0001000	1000	1.3600	1	5	< 1
uniform-0001000-2	1000	1.3782	1	5	< 1
fpg-poly-0000001000	1000	1.3498	26	44	< 1
uniform-0001000-1	1000	1.3699	19	36	< 1
euro-night-0001000	1000	1.3750	1	30	< 1
pntset-0001000	1000	1.3887	1	25	< 1
paris-0001000	1000	1.3721	13	27	< 1
pr1002	1002	1.4142	1	5	< 1
u1060	1060	1.4142	1	4	< 1
xit1083	1083	1.4142	1	16	< 1
vm1084	1084	1.3969	1	7	< 1
fpg-poly-0000001100	1100	1.3605	29	53	< 1
pcb1173	1173	1.3959	13	36	< 1
fpg-poly-0000001200	1200	1.3626	18	32	< 1
d1291	1291	1.4142	1	8	< 1
fpg-poly-0000001300	1300	1.3702	53	74	1
rl1304	1304	1.3844	111	140	3
rl1323	1323	1.4137	1	12	< 1
dka1376	1376	1.4142	1	10	< 1
nrv1379	1379	1.3731	16	32	< 1
dca1389	1389	1.4000	46	65	2
fpg-poly-0000001400	1400	1.3959	1	2	< 1
fl1400	1400	1.4142	1	1	< 1
u1432	1432	1.4142	8	18	3
dja1436	1436	1.4142	1	12	< 1
icw1483	1483	1.4142	1	31	1
fra1488	1488	1.4142	1	6	< 1
fpg-poly-0000001500	1500	1.3545	63	96	2
fl1577	1577	1.4142	1	1	5
rbv1583	1583	1.4000	44	73	3
rby1599	1599	1.4000	36	65	3
fpg-poly-0000001600	1600	1.3705	58	85	2
fnb1615	1615	1.4142	1	12	< 1
d1655	1655	1.4142	1	1	< 1
fpg-poly-0000001700	1700	1.3457	60	85	3
vm1748	1748	1.3964	1	39	3

instance	n	ρ	#full dil.	#sampled dil.	BINMDT time (s)
djc1785	1785	1.4142	1	17	< 1
fpg-poly-0000001800	1800	1.3742	115	145	5
u1817	1817	1.4142	1	1	< 1
rl1889	1889	1.4142	1	10	1
fpg-poly-0000001900	1900	1.3768	96	121	5
dcc1911	1911	1.4142	1	18	< 1
dkd1973	1973	1.3540	92	123	8
euro-night-0002000	2000	1.3518	145	193	8
pntset-0002000	2000	1.3812	1	9	< 1
uniform-0002000-1	2000	1.3700	16	38	1
uniform-0002000-2	2000	1.3644	18	42	1
paris-0002000	2000	1.3754	53	83	3
skylake-0002000	2000	1.3680	29	62	2
fpg-poly-0000002000	2000	1.3631	40	70	3
us-night-0002000	2000	1.3745	63	105	5
djb2036	2036	1.4142	1	24	1
dcb2086	2086	1.4142	1	6	< 1
fpg-poly-0000002100	2100	1.3544	125	177	9
d2103	2103	1.4142	1	155	39
bva2144	2144	1.4142	1	9	< 1
u2152	2152	1.4142	61	109	14
xqc2175	2175	1.4142	1	9	< 1
fpg-poly-0000002200	2200	1.3666	71	113	5
bck2217	2217	1.4142	1	8	< 1
fpg-poly-0000002300	2300	1.3732	128	170	9
xpr2308	2308	1.4142	1	5	< 1
u2319	2319	1.4142	1	1	< 1
ley2323	2323	1.3720	43	102	7
dea2382	2382	1.4142	1	45	3
pr2392	2392	1.4142	1	3	< 1
fpg-poly-0000002400	2400	1.3797	81	122	7
rbw2481	2481	1.4142	1	24	2
fpg-poly-0000002500	2500	1.3656	109	150	9
pds2566	2566	1.3686	95	127	13
mlt2597	2597	1.3868	130	182	18
fpg-poly-0000002600	2600	1.3647	114	154	10
fpg-poly-0000002700	2700	1.3729	125	172	12
bch2762	2762	1.4142	1	12	1
fpg-poly-0000002800	2800	1.3670	109	147	11
irw2802	2802	1.4142	1	9	< 1
lsm2854	2854	1.4142	1	28	2
fpg-poly-0000002900	2900	1.3945	66	123	10
dbj2924	2924	1.4142	1	7	< 1
xva2993	2993	1.4142	1	8	< 1
fpg-poly-0000003000	3000	1.3758	133	177	16
uniform-0003000-1	3000	1.3756	46	77	6
euro-night-0003000	3000	1.3746	194	247	22

instance	n	ρ	#full dil.	#sampled dil.	BINMDT time (s)
pntset-0003000	3000	1.3818	36	71	5
skylake-0003000	3000	1.3839	53	93	7
uniform-0003000-2	3000	1.3864	23	57	4
us-night-0003000	3000	1.3664	169	243	23
paris-0003000	3000	1.3655	118	173	15
pcb3038	3038	1.4142	1	14	< 1
pia3056	3056	1.4142	1	32	3
dke3097	3097	1.4142	1	46	3
fpg-poly-0000003100	3100	1.3549	112	161	15
lsn3119	3119	1.4142	1	9	< 1
lta3140	3140	1.4142	1	6	< 1
fpg-poly-0000003200	3200	1.3695	127	170	17
fdp3256	3256	1.4142	1	7	< 1
beg3293	3293	1.3955	297	462	80
fpg-poly-0000003300	3300	1.3903	115	152	17
dhb3386	3386	1.4142	1	21	2
fpg-poly-0000003400	3400	1.3735	126	175	19
fpg-poly-0000003500	3500	1.3795	157	204	24
fpg-poly-0000003600	3600	1.3732	146	205	25
fjs3649	3649	1.4142	1	5	< 1
fjr3672	3672	1.4142	1	5	< 1
dlb3694	3694	1.4142	1	21	2
fpg-poly-0000003700	3700	1.3741	221	284	36
ltb3729	3729	1.4142	1	6	< 1
fl3795	3795	1.4142	1	1	52
fpg-poly-0000003800	3800	1.4038	1	98	8
xqe3891	3891	1.4142	1	5	< 1
fpg-poly-0000003900	3900	1.3691	133	191	27
xua3937	3937	1.4142	1	2	< 1
dkc3938	3938	1.4142	1	20	2
dkf3954	3954	1.4142	1	98	7
paris-0004000	4000	1.3629	147	214	30
uniform-0004000-2	4000	1.3942	51	99	13
us-night-0004000	4000	1.3902	176	231	38
fpg-poly-0000004000	4000	1.3658	223	351	55
euro-night-0004000	4000	1.3761	171	215	38
pntset-0004000	4000	1.3874	51	109	14
skylake-0004000	4000	1.3970	1	21	2
uniform-0004000-1	4000	1.3668	49	93	11
fpg-poly-0000004100	4100	1.3789	165	209	33
fpg-poly-0000004200	4200	1.3848	149	202	37
fpg-poly-0000004300	4300	1.3634	225	298	50
bgb4355	4355	1.4142	1	9	< 1
bgd4396	4396	1.4142	1	30	3
fpg-poly-0000004400	4400	1.3998	131	181	33
frv4410	4410	1.4142	1	35	3
fnl4461	4461	1.4084	15	34	5

instance	n	ρ	#full dil.	#sampled dil.	BINMDT time (s)
bgf4475	4475	1.3868	203	269	81
fpg-poly-0000004500	4500	1.3754	171	239	46
fpg-poly-0000004600	4600	1.3669	217	275	60
fpg-poly-0000004700	4700	1.3901	195	251	52
fpg-poly-0000004800	4800	1.3859	171	234	52
fpg-poly-0000004900	4900	1.3983	1	225	46
xqd4966	4966	1.4142	1	8	< 1
pntset-0005000	5000	1.3846	50	104	20
skylake-0005000	5000	1.3791	109	182	38
fpg-poly-0000005000	5000	1.3771	268	326	78
uniform-0005000-1	5000	1.3871	53	97	18
euro-night-0005000	5000	1.3880	278	338	84
us-night-0005000	5000	1.3717	322	408	104
uniform-0005000-2	5000	1.3760	68	122	25
paris-0005000	5000	1.3818	171	237	54
fqm5087	5087	1.4142	1	23	3
fpg-poly-0000005100	5100	1.3692	233	296	74
fpg-poly-0000005200	5200	1.3853	1	9	1
fpg-poly-0000005300	5300	1.3687	243	314	84
fpg-poly-0000005400	5400	1.3686	261	343	104
fpg-poly-0000005500	5500	1.3844	292	365	106
fea5557	5557	1.4142	1	16	3
fpg-poly-0000005600	5600	1.4035	1	211	62
fpg-poly-0000005700	5700	1.3937	218	267	84
fpg-poly-0000005800	5800	1.3847	286	359	114
fpg-poly-0000005900	5900	1.3864	192	258	82
rl5915	5915	1.4142	1	34	9
rl5934	5934	1.4142	1	7	3
uniform-0006000-1	6000	1.3929	59	126	35
skylake-0006000	6000	1.3940	106	188	55
us-night-0006000	6000	1.3884	307	380	133
uniform-0006000-2	6000	1.3832	56	126	32
fpg-poly-0000006000	6000	1.3811	207	283	106
euro-night-0006000	6000	1.3776	485	567	208
world-0006000	6000	1.3805	500	591	237
pntset-0006000	6000	1.3787	68	134	36
fpg-poly-0000006100	6100	1.3940	130	188	64
fpg-poly-0000006200	6200	1.3727	289	366	137
fpg-poly-0000006300	6300	1.3880	273	363	145
fpg-poly-0000006400	6400	1.3796	342	432	168
fpg-poly-0000006500	6500	1.3693	355	452	206
fpg-poly-0000006600	6600	1.3790	234	321	129
fpg-poly-0000006700	6700	1.3947	192	260	116
fpg-poly-0000006800	6800	1.3663	317	433	186
xsc6880	6880	1.4142	1	26	4
fpg-poly-0000006900	6900	1.3795	265	350	170
uniform-0007000-1	7000	1.3672	55	133	43

instance	n	ρ	#full dil.	#sampled dil.	BINMDT time (s)
euro-night-0007000	7000	1.3844	422	522	263
uniform-0007000-2	7000	1.3868	80	147	55
skylake-0007000	7000	1.3854	169	253	104
us-night-0007000	7000	1.3776	622	749	370
pntset-0007000	7000	1.3919	61	144	53
fpg-poly-0000007000	7000	1.3818	301	393	185
world-0007000	7000	1.3699	557	667	330
fpg-poly-0000007100	7100	1.3897	218	297	134
bnd7168	7168	1.4142	1	27	5
fpg-poly-0000007200	7200	1.3851	287	379	188
fpg-poly-0000007300	7300	1.3786	346	443	248
pla7397	7397	1.4142	1055	1098	6502
fpg-poly-0000007400	7400	1.3812	560	656	357
lap7454	7454	1.4142	1	49	9
fpg-poly-0000007500	7500	1.3864	291	379	204
fpg-poly-0000007600	7600	1.3859	312	407	224
fpg-poly-0000007700	7700	1.3737	349	448	285
fpg-poly-0000007800	7800	1.3790	302	391	227
fpg-poly-0000007900	7900	1.3878	232	324	190
fpg-poly-0000008000	8000	1.3996	327	454	279
pntset-0008000	8000	1.3897	102	178	85
us-night-0008000	8000	1.3791	595	694	444
world-0008000	8000	1.3793	616	765	493
uniform-0008000-2	8000	1.3924	66	138	64
jupiter-0008000	8000	1.3700	611	723	449
euro-night-0008000	8000	1.3909	432	547	386
uniform-0008000-1	8000	1.3956	90	197	90
fpg-poly-0000008100	8100	1.3880	353	454	286
ida8197	8197	1.4142	1	10	2
fpg-poly-0000008200	8200	1.3790	311	397	252
fpg-poly-0000008300	8300	1.3718	331	464	294
fpg-poly-0000008400	8400	1.3885	294	411	261
fpg-poly-0000008500	8500	1.3823	281	485	324
fpg-poly-0000008600	8600	1.3791	406	519	363
fpg-poly-0000008700	8700	1.3777	328	450	328
fpg-poly-0000008800	8800	1.4029	346	440	325
fpg-poly-0000008900	8900	1.3835	387	525	399
world-0009000	9000	1.3723	621	746	591
jupiter-0009000	9000	1.3971	408	497	402
euro-night-0009000	9000	1.3864	904	1245	1053
fpg-poly-0000009000	9000	1.3911	308	403	303
pntset-0009000	9000	1.3883	75	131	74
us-night-0009000	9000	1.3802	468	568	459
uniform-0009000-2	9000	1.3896	87	179	111
uniform-0009000-1	9000	1.3895	90	191	122
fpg-poly-0000009100	9100	1.3823	268	411	318
fpg-poly-0000009200	9200	1.3812	341	466	362

instance	n	ρ	#full dil.	#sampled dil.	BINMDT time (s)
fpg-poly-0000009300	9300	1.3922	299	401	331
fpg-poly-0000009400	9400	1.3789	416	509	468
fpg-poly-0000009500	9500	1.3927	369	491	420
fpg-poly-0000009600	9600	1.3951	307	401	348
dga9698	9698	1.4142	1	16	4
fpg-poly-0000009700	9700	1.3712	417	608	548
fpg-poly-0000009800	9800	1.3896	389	487	447
fpg-poly-0000009900	9900	1.3836	512	646	687
euro-night-0010000	10000	1.3868	462	601	577
uniform-0010000-2	10000	1.3756	107	197	138
world-0010000	10000	1.3973	519	651	727
uniform-0010000-1	10000	1.3811	133	244	195
pntset-0010000	10000	1.4079	90	187	136
jupiter-0010000	10000	1.3888	618	786	773
fpg-poly-0000010000	10000	1.3861	455	584	556
us-night-0010000	10000	1.3859	397	515	502

■ **Table 4** Solutions and runtimes for *public* benchmark set together with the number of full and sampled dilation computations that are the bottleneck in the exact algorithm. The presented data was obtained using the binary solver with an improved delaunay triangulation as an initial solution.